Numerical Study of Wave Run-up on Semi-submersible Platforms

By

Dongsoo Kim

Submitted for the Degree of master of Philosophy

Department of Naval Architecture and Marine Engineering

University of Strathclyde

August 2018

Declaration of Authenticity and Author's Rights

This thesis is the result of the author's original research. It has been composed by the author and has not been previously submitted for examination which has led to the award of a degree.

Signed:

Date:

Acknowledgements

I would first like to thank my supervisors Prof. Atilla Incecik from the Department of Naval Architecture and Marine Engineering at the University of Strathclyde. He consistently allowed this paper to be my own work but provided me with the research environment I needed. I also wish to express my thanks to my Korean supervisor Prof. Kwang-hyo Jung of the Department of Naval Architecture and Ocean Engineering at Pusan National University. He supported me to have the opportunity to study at the University of Strathclyde.

I would also like to thank Dr. Tahsin who helped me with computational environment. Without his enthusiastic assistance, the simulation would not have been successful. My sincere thanks also go to Mr. Byongug Jeong who was kindly willing to give the chance to use his personal computer to run lots of simulations efficiently.

Finally, I must express my profound gratitude to my parents who have brought up me to come to this place and to my only younger brother who has filled my place by my parents, and to my girlfriend who has been waiting for me without complaining for their heartfelt interest and continuous encouragement throughout my year of research. This achievement would never have been possible without them.

Sincerely Thanks to all.
Dongsoo Kim

Abstract

For designing new floating platforms, the model tests in wave tank are carried out to investigate hydrodynamic properties and other parameters during design process. However, even though these experiments are able to help researchers with understanding the physical meaning directly, it has naturally made it to spend lots of time including from manufacturing test model to using the test facilities.

The motions and flow characteristics of a floating hull are closely associated with nonlinearity of incident, reflected and scattered waves, which have undoubtedly made hydrodynamic problems complicated and challenging. The waves around a structure can be amplified by their interaction with the structure and wave to wave interactions, which lead to even higher and steeper wave crests.

In the present study, through comparisons, the main purposes are to understand physical mechanisms of wave run-up phenomenon with relevant parameters. The numerical simulations were performed using the Volume of Fluid (VOF) method in Computational Fluid Dynamics (CFD) using the commercial software Star-CCM+. In order to validate this work's CFD results, existing experimental data from the open literature were investigated. The simulated wave run up results of a rigidly fixed semi-submersible geometry were compared against published experiment data, with SESAM program. The influence of higher-order wave components could be investigated by directly comparing both results. Also, for the quick calculations, wave run-ups with different hull displacements were used to derive a simplified estimation formula using wave parameter and column diameter. Lastly, the survival draft conditions were added to compare with existing operational draft condition. In general, it was found that low draft and high frequency were the main factors influencing the results, particularly in the aft column. In conclusion, this work's CFD results are in reasonably good agreement with experiments and therefore the CFD technique can provide useful guidance for designing platforms in this field.

Key words: Wave run-up, Regular wave, Computational Fluid Dynamics (CFD), Semi-submersible platform, Potential flow theory

Contents

List of Tables

List of Figures

1 Introduction

In recent years, the demand for oil and gas has begun to increase gradually after suffering a recession by the shale gas. In design stage, the impact loading due to waves is one of the most significant design factors for ship, offshore and coastal structures ranging from operational to extreme conditions. Especially, for offshore platforms, the distance between the lowest deck and maximum water level (so called air gap) has been acknowledged as an issue of concern over a few decades or so. This is due to the fact that there has been a still challenge for estimating free surface elevation around large volume structures in steep waves. Therefore, the accurate prediction of both air gap and local wave amplification is extremely essential for engineers to reduce the wave-in-deck impact and damage to the floating offshore systems such as a semi-submersible during its expected life.

Designing the floater having higher deck height with an unnecessary air gap seems to have some limitations due to weights, building costs and stability requirements. Thus, it needs to be paid much attention to determine static air gap with complicated wave-columns interaction problem since the hydrodynamic problem is intrinsically demanding and inherently difficult tasks.

Figure 1.1 Wave run-up phenomenon

As can be seen in Figure 1.1 that the wave run-up phenomenon is the vertical uprising of water that is a result of an incident wave train breaking on a bluff body. The wave run-up can result in a variety of wave impact hazards acting on the structure later on.

For instance, they are wave-in-deck loads and further green water phenomenon that have attracted much interests from around the world. In order to investigate the wave run-up in floating units which have multiple columns geometry, the platform motions are usually analysed with both radiation and diffraction effects. In the present study, it should be noted that the non-linear effects related to interaction between columns and waves including incident, reflected would be significant.

Among numerous offshore platforms, a semi-submersible is one of the typical floating offshore structures used for drilling rigs, safety vessels and oil production platform. It has been good for having good sea-keeping and ballasting capacity with ship-shaped underwater pontoon compared to normal ship.

Model scale tests are conducted at the final stages of the design to verify the various hydrodynamic coefficients and behaviour of the system, but the experimental approach is not often practical at the early stages. Therefore, the use of CFD technologies that can estimate the value of parameters from the vicinity of the structure has been become attractive and popular. The CFD tool used in this study is Star-CCM+ software of SIEMENS based on Navier-Stokes equations, in where VOF method is applied on evolution of free surface. Moreover, a new technique, wave forcing method was used for elimination of numerically reflected waves and the efficiency of time.

The Star-CCM+ numerical simulation results of the wave run-up along the columns of a rigidly fixed semi-submersible platform are main topic of this research. The analysis was carried out so as to verify discrepancies between wave elevation predictions based on linear diffraction analysis and numerically calculated values. Also, a simple estimation equation for wave run-up height was derived from some different hull volume displacement of the semi-submersible model. In addition, the wave run-up effects of draft and pontoon on this phenomenon were investigated by adding two more reduced draft that can be considered as a survival condition and further were discussed.

2 Objectives

Instead of physical test in wave basin, a number of numerical methods have been recently developed to predict the wave run-up around columns and to compare with the experimental data in offshore structures field. These methods can be roughly categorized into computational method (nonlinear) and diffraction analysis method (1st or 2nd order). As a typical example, WAMIT is one of the numerical codes based on potential theory, which enables even second-order for nonlinearities to be analysed. Other than this, many hydrodynamic in-house codes have been used to predict wave elevation and body motion in various universities and research organizations. Since the most of the codes described above are based on linear or second-order wave theory, they cannot consider fully non-linear effects and are therefore easy to underestimate the values, especially for waves with steep slopes. Instead, they have advantage of the relatively less computer CPU times to complete the calculations rather than using fully non-linear tools.

The aim of this present research is to contribute to enhancing hydrodynamic simulations using CFD for semi-submersible platform. With CFD, Wadam was used to demonstrate the effects of higher-order wave components on wave run-up values close to columns. To achieve this, the following objectives are set up;

● To overview trend of a wave run-up phenomenon, previously conducted numerical methods to review their limitations and to identify where to be improved.

● To basically study wave run-up around column of a fixed semi-submersible with fully nonlinear tool (CFD) and linear analysis (Wadam) based on potential flow model.

● To investigate wave run-up on a semi-submersible model with the different hull displacement and examine the effects of draft.

● To provide recommendations for future research.

3 Literature Review

3.1 Introduction

In this section, it largely outlines two approaches: experimental method and numerical method. In the part of the experiment, it briefly indicates the general trend of experiments about cylindrical or full-scaled floating model which have been conducted in wave tank. In the other section, it discusses current computational technologies for closely investigating wave run-up phenomenon around column.

3.2 Numerical Studies

Several numerical studies have been performed to estimate the wave run-up around a circular column. Firstly, a second-order boundary element model was used to calculate wave run-up under interaction between waves, current and a structure (Büchmann et al., 1998). A fully nonlinear numerical method was applied a fully nonlinear numerical method for calculating wave scattering around fixed vertical truncated cylinder and compared with linear and second-order results, as well as with experiments. (Trulsen and Teigen, 2002). The air gap was extensively investigated under floating platforms and run-up along columns which is part of the work of ISSC2000 Committee (Nielsen, 2003). A number of linear and non-linear radiation–diffraction programs were employed from various individuals and organizations to see how well they are able to calculate the air gap and run-up, comparing experimental results. The used codes all are based on potential theory and have different characteristics for each case such as the truncated circular column, rectangular column that has round corner and complete semi- submersible model.

The numerical methods was used using the WAMIT program based on 1st and 2nd-order diffraction analysis to compare with experiment conducted in MARINETEK (Kristiansen et al., 2004); They found that some discrepancy between measurements

and numerical results, which appeared to be caused by high-order non-linear terms. In another paper, the run up elevation in diffracted wave around a single, fixed cylinder were compared to second order potential theory (WAMIT) and commercial CFD code, Flow-3D (Kristiansen et al., 2005). Similar to the research described earlier, WAMIT and ComFLOW (CFD) were compared with the experiments, which are observed to depend on incident wave steepness and wave length. In addition to regular waves, irregular sea conditions were also used for studying wave run-up effects (Danmeier et al., 2008).

The open source codes of OpenFOAM were utilized to monitor wave elevations around a fixed vertical cylinder. Measured locations were within a radial distance. Thus, the results of wave run-up and scattering were compared with physical tests (Cao et al., 2011). The Modified Marker-Density (MMD) method was utilized to numerically simulate wave run-up around a circular column (Yang et al., 2015). The flow phenomenon around a vertical circular cylinder was simulated to compare both the wave run-up height in front of it and depression depth at the back with previous published experimental data as well as values obtained from Bernoulli's equation (Xiao et al., 2016); The commercial CFD solver, Star-CCM+ was used to conduct this numerical simulation depending on Froude number. It was found that run-up height and depression depth increased with increasing Fr number except that at high Fr number, the CFD results and measurement data were less than the theoretical values. Also, wave run-up simulations around a circular cylinder were performed with Star-CCM+ (Cha et al., 2016).

The CFD simulation of wave run-up on a large deep draft floating platform which has been known as spar was carried out using Fluent CFD software. The simulation results have been validated with the expected results from empirical method (Repalle et al., 2007). The CFD simulations (ComFLOW) of wave run-up on a half-shaped semi-submersible were compared with measured results for regular wave conditions (Iwanowski et al., 2009); The pressure and velocity at several locations on the columns were recorded and the pressure time history was directly compared with experimental data. Overall, it has shown that this numerical method can be utilised to capture the highly non-linear flow of wave run-up.

The tests were conducted about a large-volume semi-submersible platform for wave run-up and air gap prediction under action of regular waves in both fixed and moored conditions (Matsumoto et al., 2013); The wave elevations measured in various locations under the deck were compared with the numerical methods. In terms of WAMIT, second order diffraction analysis as well as standard linear analysis was used to calculate the values, with fully non-linear using ComFLOW for only fixed case. The values obtained from both second order and simulation have relatively shown good agreements with experimental data. Also motion in moored test has favourably reduced the wave run up magnitude even in the region where there is large amplification in fixed one.

The experimental study of wave run-ups on a scaled, fixed and half-shaped semi-submersible was carried out in wave basin (Kim et al., 2014); Under the regular wave, the two different draft (operational & survival) were considered and then the results of wave run-ups were compared with numerical results based on potential flow analysis in frequency domains. It was observed that when determine the air gap, non-linear run-up characteristic should be carefully taken into account in a low draft and short period condition.

The wave run-up and impact load on a moored semi-submersible under an extreme wave condition using Star-CCM+ CFD software were studied (Lee et al., 2014); Its equivalent regular wave as well as the random wave of 100-year return period in the Gulf of Mexico (GOM) was employed to model environmental wave. The impact pressure in regular cases seemed to be slightly higher than that in random waves. Furthermore, the surge and heave motions in phase with extreme wave crest played an important role in both reduction of impact load and secure of air-gap.

The global motion and air gap for a semi-submersible floating unit in terms of hydrodynamics using potential flow theory were investigated with various aspects (Zhang et al., 2017); The wave heading directions were varied with different conditions such as short and long-crested waves. Also, the response amplitude operator (RAO) depending on the variation of the principal dimensions of the semi-submersible was systematically analysed to investigate the influence of the motion and optimize the hull form later.

In general, the previous numerical approaches have mainly focused on comparisons with the experimental, theory and potential method. As projected, the numerical method has the advantage of time efficiency and is good at approximating actual experimental values. Although there was a study of air gaps and motion with varying dimensions of a semi-submersible, there has not been even simple equation for run-up heights. Thus, in this thesis, an expression for estimating rough run-up values from displacement models of different sizes would be derived under regular wave condition. Basically, of course, like any other related paper, analyses through potential theory will be performed to comprehend wave run-up phenomenon clearly.

3.3 Experimental Studies

Many studies have been carried out to investigate wave run-up phenomenon through an experimental method. The models used in test have had a wide range of shape from the classical circular cylinder to offshore structures which have single or multi-columns. Most of experimental studies have been focused on measuring local wave amplification around cylinder and near the column under the deck of structure. For a ratio of the column diameter to the incident wave length of greater than 0.2, diffraction theory should be considered to predict wave run-up along the column.

An analytic solution was suggested which is based on linear potential theory in diffraction problem for single bottom-mounted column under regular waves. (McCamy and Fuchs, 1954). Experiments were carried out to predict wave run-up at side of the cylinder through both single thin pile and pile groups (Haney and Herbich, 1982); It was found that velocity head using Dean stream function theory can be used to calculate design run up with scattering parameter that is composed of wave number and cylinder radius.

The wave run-up and forces applied on a bottom mounted cylinder in regular and random waves were studied and it was found that linear diffraction theory tended to predict the wave run-up heights less than measured those except for very low wave

steepness (Niedzwecki and Duggal, 1992). Also, the wave interaction in tension leg platform was investigated in terms of both wave run-up on a leg and wave amplification beneath the deck (Niedzwecki and Huston, 1992); The wave run-ups were compared with three different column spacing in this TLP structure with both with and without pontoon. As the column spacing decreased, the wave run-up on aft column rose, especially with the pontoon. This study also showed that local wave height has nearly doubled in regular wave.

A method to compute the wave run-up of the large cylinder under non-linear regular and irregular waves was developed (Kriebel, 1993); The regular wave was decomposed so that linear diffraction theory can be applied to each wave component including higher order and was summed as superposition. This method was also extended to narrow band irregular wave later. The run-up experiments on a cylinder were carried out for surface gravity waves and analysed in terms of harmonic components (Morris-Thomas and Thiagarajan, 2004); They also realized that second-order diffraction theory is not enough to account for complete wave run-up.

In the case of platform model experiment, the tests with a scaled model of Heidrun TLP for regular waves were conducted to examine how the variations in relevant parameters, such as wave frequency, height and incoming wave angle affect the run up as well as jetting phenomenon (Arnott et al., 1998). It was concluded that the steep wave made the wave run up significant and the wave with the largest height resulted in up to 2-fold amplification.

The relative wave amplification under a large semi-submersible for random waves (two sea states) was investigated in tests where the model had the motions such as heave, roll, pitch. The incident wave direction was also varied from head, oblique, beam seas (Kriebel); It showed that wave amplification could be increased when compared to the incident wave in some locations under and around the model.

The experimental study of the evaluation of the air gap of semi-submersible model in both restrained and moored configuration was performed to operate in Brazil's Campos Basin (Simos et al., 2006); A set of regular wave and storm-sea condition were used to observe the free surface elevation at some wave probes under the deck. Thus, wave elevations and RAOs (heave and pitch) obtained from standard linear

analysis using WAMIT were compared to those measured physically. It is noted that the design of deck region close to the column walls should be taken more cares since there was significant non-linear wave run-up effect (especially for steep wave), specifically in front of the stern column in this type of platform.

As a similar experiment, the physical model tests on a semi-submersible were performed in heading regular wave with both fixed and moored (free to oscillate) conditions. At different locations underneath its deck, wave elevations were measured and analysed with motion effect (Kazemi and Incecik, 2006) (Shan et al., 2011); Kazemi (2006) also measured the vertical impact loads in case of having negative air gap, which showed that it was highly dependent on wave steepness. As common results, the amount of wave run-up elevation was highly associated with wave steepness and reduced considerably when it is free to respond to the waves in spite of severe wave non-linearity.

To summarize the previous experiments explained earlier, there have been numerous studies on wave run-up of offshore structure. Especially, a floating condition actually seems reasonable to investigate the phenomenon and experiments are being conducted accordingly. Before starting these kinds of floating physical tests, the most important point is that mooring conditions should be properly modelled with considering chain properties. This may further improve understanding of the combined actions and effects of motion and mooring. Although no direct test was performed in this study, many reviews of the papers regarding run-up experiment enabled to identify the research trends and directions.

3.4 Summary

Most of the numerical approaches conducted have been focused on the computer-based CFD and 1^{st} or 2^{nd} order diffraction theory based method. Each method has advantages and disadvantages in terms of the calculation accuracy and CPU time etc. In the present study, a comparison of CFD simulation and linear (1^{st} order) diffraction will be made basically to understand the wave run-up phenomenon around column and

will further analyse its effect according to change in hull displacement. Thus, the overall analysis carried out in this research can be briefly summarized as below:

● The validation of regular wave elevation profile (without model) with Stokes 5th wave theory using CFD (Star-CCM+) before wave run-up simulations.

● The validation with CFD (Star-CCM+) for predicting the wave run-up elevation in the vicinity of the fore and aft columns of a semi-submersible model under heading regular wave with the model restrained.

● The comparison of wave run-up elevation at certain points depending on different wave frequency and steepness for heading regular waves using Star-CCM+ (fully nonlinear) and Wadam (1st order diffraction analysis).

● The investigation on wave run-up variation with varying hull displacement of basic semi-submersible model and obtain a design formula for estimating wave run-up height to some extent.

● The comparison of the previous draft plus two different draft conditions in the displacement model having the most critical wave run up values, with pontoon effect.

This dissertation is organised as follows: Chapter 1 is introduction. In Chapter 2, the aim of this study is described in depth. Chapter 3 is devoted to explain numerical and experimental researches which have been studied previously. Chapter 4 contains numerical model including some mathematical concepts, the governing equations, and wave forcing method etc. Chapter 5 shows that experimental model conditions from reference paper. In Chapter 6, for validation cases, the computational set-up as well as the results of wave elevation and wave run-up are easily presented with several schematic views. Chapter 7 represents hydrodynamic set-up and panel convergence test in Wadam. Chapter 8 presents the results of wave run-up RAOs obtained from two different methods to discuss nonlinear (higher-order) effects (Part 1) under heading regular wave conditions. In addition, Part 2 shows the difference of the wave run-up values with varying semi-submersible hull displacement, and further with draft changes (Part 3), concluding mentions in Chapter 9 (Chapter 10 contains desirable future works).

4 Methodology

4.1 Introduction

This section describes the methodology of this research. Basically, Computational Fluid Dynamics (CFD) based on Finite Volume Method (FVM) is used with RANS, VOF, SIMPLE and wave focusing method. Therefore, this section explains overall definition of the computational methods, RAOs from existing frequency domain analysis and even the equation of motion in a floating body as reference material.

4.2 Equation of Motion

The equation of motion can be basically achieved by applying Newton's law and including the added mass, damping and exciting force acting on the structure. Therefore, the equation of motion of ships and offshore structures is generally as follows:

$$\left(M + a_{ij}\right)\ddot{X} + \left(b_{ij} + b_v\right)\dot{X} + cX = F$$

where M is mass of the structure, a_{ij} is the added mass, b_{ij} is the linear damping coefficient, b_v is also damping coefficient caused by fluid viscosity, c is the restoring force and F is the exciting wave force.

In this study, the one of the programs in Sesam, Wadam solves the harmonic motion of rigid body systems based on the hydro panel model in the frequency domain for a given incident wave frequency ω and heading angle β. Furthermore, the eigenvalues and eigenvectors obtained from the eigenvalue problem are used to calculate the natural period of the rigid body.

4.3 Velocity Potential

In global response analysis, since the potential flow theory is used to calculate the motions of the platform and wave forces acting on it, it is should be noted that the velocity potential equation can be written as below:

$$\emptyset(x,y,z) = Re[\emptyset(x,y,z)]e^{i\omega t}$$

$$\emptyset(x,y,z) = \frac{gA}{i\omega}\{\phi_I(x,y,z) + \phi_s(x,y,z)\} + \sum_{J=1}^{6} i\omega\, X_J\phi_J(x,y,z)$$

where g is the gravity acceleration, A is the incident wave amplitude, X_J is the motion amplitude, ϕ_I is incident wave potential, ϕ_s is scattering wave potential, ϕ_J is the radiation wave potential and J is defined as the motion direction (6-DOF). According to the equation above, in the incident and scattered wave, the amplitude and phase are assumed to be the same while the radiation term is usually different depending on the motions. Also, the radiation terms in each motion can be summed to obtain the total radiation wave.

4.4 Relative Wave Elevation

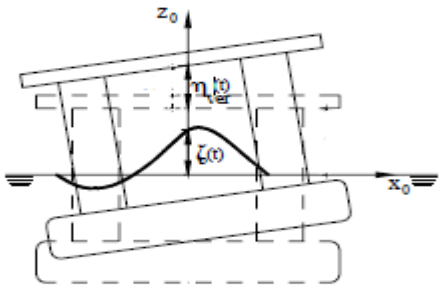

Figure 4.1 Schematic view of the floating model in wave

(Kazemi and Incecik, 2006)

The concept of relative wave elevation is firstly explained as background information. Unlike a fixed condition used in the present study, especially, in a floating condition, wave elevation relative to the motions should be considered. A schematic view of the semi-submersible under the wave is illustrated in Figure 4.3. At the field point of interest underneath deck bottom (x, y, t), the relative wave surface elevation $\zeta_{rel}(t)$ in the frame of reference of the model can be expressed as follows:

$$\zeta_{rel}(t) = \zeta(t) - \eta_{ver}(t)$$

where $\zeta(t)$ denotes the absolute wave elevation with respect to a fixed condition from still water level (SWL), $\eta_{ver}(t)$ is the vertical displacement due to the combined motion that generally includes heave, roll, pitch, which can be computed by:

$$\eta_{ver}(t) = \eta_3(t) + y\eta_4(t) - x\eta_5(t)$$

Where in $\eta_i(t)$, the number 3, 4, and 5 mean the platform motions of the heave, roll and pitch, respectively. As aforementioned, the relative wave elevations in moored (floating) conditions can be calculated from the formula. On the other hand, the $\eta_{ver}(t)$ is undoubtedly zero without any motions for fixed one, which will be of our main interest soon. The $\zeta_{rel}(t)$ will naturally mean the absolute wave elevation $\zeta(t)$.

4.5 Governing Equations (RANS)

This chapter explains the computational fluid dynamic numerical methodology to obtain adequate solutions. In this study, the fluid flow can be found by solving continuity equations which basically represent mass conservation in the domain. Also, the CFD calculations are based on simulated solutions to the Reynolds Averaged Navier-Stokes (RANS) equations describing conservation of momentum, performed using Star-CCM+ software based on Finite Volume Method (FVM). In other words, the two governing equations described above are solved in each mesh or grid, called control volume which forms a computational domain together. The continuity and the RANS equations for 3-dimensional incompressible turbulent flows can be expressed, respectively as follows:

$$\frac{\partial u_i}{\partial x_i} = 0$$

$$\frac{\partial}{\partial t}(\rho u_i) + \frac{\partial}{\partial x_i}(\rho u_i u_j) = -\frac{\partial p}{\partial x_i} + \frac{\partial}{\partial x_j}\left[\mu\left(\frac{\partial u_i}{\partial x_j} + \frac{\partial u_j}{\partial x_i}\right)\right] + \frac{\partial}{\partial x_j}(-\rho\overline{u_\iota u_j})$$

Where $u_i = (u, v, w)$ is defined as fluid velocity, $x_i = (x, y, z)$ is direction in the Cartesian coordinate, ρ is the density of fluid, p is pressure, μ is the dynamic viscosity coefficient of the fluid and $(-\rho\overline{u_\iota u_j})$ is the Reynolds stress. In detail, the transportation equation of the Reynolds stress (Eq. (3)) can be expressed as below:

$$\begin{aligned}\frac{\partial}{\partial t}(\rho\overline{u_\iota u_j}) + \frac{\partial}{\partial x_k}(\rho U_k \overline{u_\iota u_j}) \\ = -\frac{\partial}{\partial x_k}(\rho\overline{u_\iota u_j u_k}) + \overline{P(\delta_{kj}u_\iota + \delta_{\iota k}u_j)} + \frac{\partial}{\partial x_k}\left[\mu\frac{\partial}{\partial x_k}(\overline{u_\iota u_j})\right] \\ - \rho\left(\overline{u_\iota u_k}\frac{\partial u_i}{\partial x_k} + \overline{u_j u_k}\frac{\partial u_i}{\partial x_k}\right) + \overline{P\left(\frac{\partial u_\iota}{\partial x_j} + \frac{\partial u_j}{\partial x_\iota}\right)} - 2\mu\overline{\left(\frac{\partial u_\iota}{\partial x_k} + \frac{\partial u_\iota}{\partial x_k}\right)}\end{aligned}$$

The main reason for using the RANS equation is to remarkably reduce the computational time when compared to a full Navier-Stokes equation that is possible by direct numerical simulation.

In order to accurately simulate the unsteady flow, the second order implicit scheme was employed for the temporal discretization and in the governing equation the diffusion(viscous) term with the second-order central difference, and the convection term with the second-upwind method were discretised in space. The used discretization setup in Star-CCM+ can be summarized in Table 4.1.

Table 4.1 Discretization setting in simulation

Term	Discretization	Order
Unsteady	Implicit	2nd
Convection	Upwind method	2nd
Diffusion	Central difference method	2nd

4.6 SIMPLE (Solution method)

For incompressible fluid flow, coupling the pressure and velocity is needed to derive a pressure equation from governing equations. The Semi-Implicit Method for Pressure-Linkage equation (SIMPLE) algorithm has been widely used to solve Navier-Stokes equations in CFD approaches. In detail, this algorithm segregates pressure correction from mass conservation and the velocity from momentum equation as separate algebraic equations, solving with linked corrector method. Briefly, this follows a guess-and-correct philosophy for the calculation of pressure through the solution of a pressure correction equation in each iteration. The general steps are described in the following diagram (Figure 4.4, CD-Adapco, 2017).

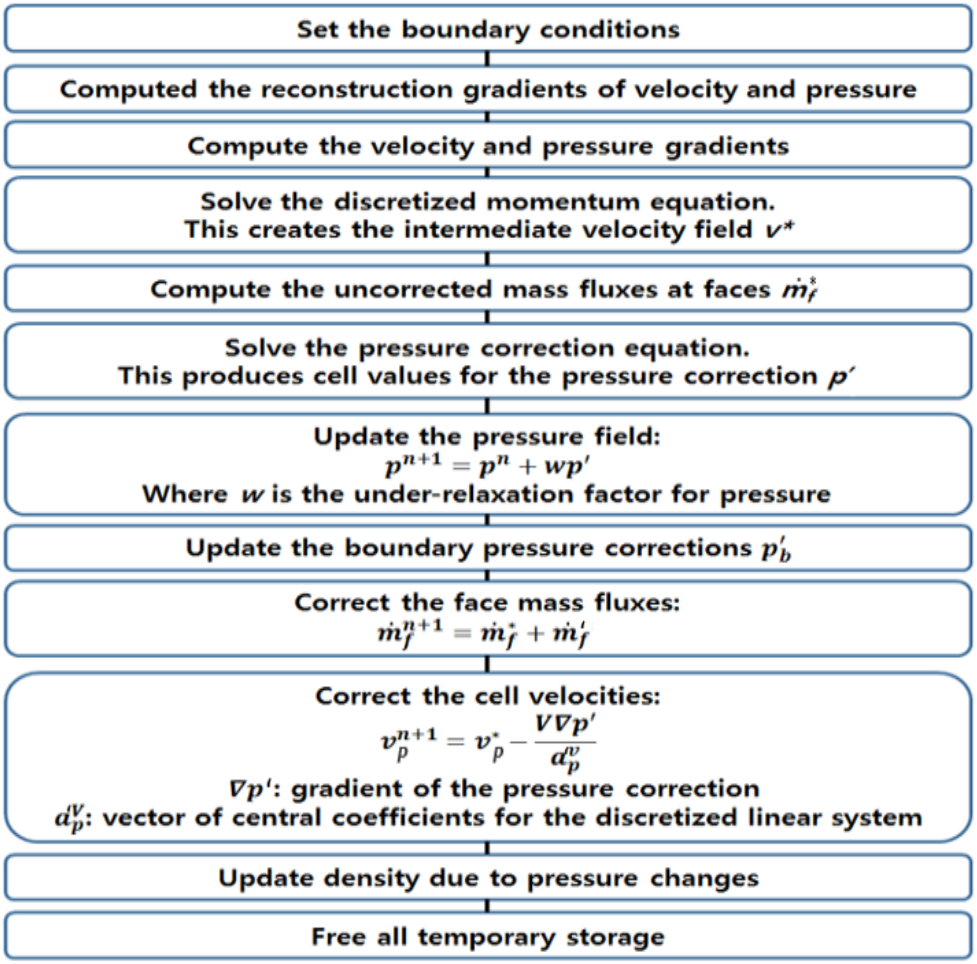

Figure 4.2 SIMPLE algorithm, adopted from CD-Adapco (2017)

4.7 Free Surface Modelling

The free surface usually means that there is immiscible, a large density difference between phases. In this simulation, the Volume of Fluid (VOF) method (Hirt and Nichols) was applied to capture the location of interface between air and water. This method has wide applications in modelling free surface flow and fluid-structure interaction. Also, when compared to dominant phases in a multiphase model, inter-phase interaction caused by contact between phases is relatively trivial, indicating that this method can be efficient in that it saves computational time. Since the VOF model is sensitive to the mesh used in simulation domain, the mesh in the region where the waves pass needs to be fine enough to reduce errors with the exact wave generation.

It introduces fractional volume of a computational grid cell which is occupied by fluid, and physical quantities such as density and molecular viscosity are calculated accordingly. In other words, the spatial distribution of each phase at a certain time is the volume fraction. The partial differential form of equation for the VOF model is described by the following equation.

$$\frac{\partial F}{\partial t} + u_i \frac{\partial F}{\partial x_i} = 0$$

where F is the volume fraction in a computation cell. The value of F varies from 0 in the air region to 1 in the water region$(0 \leq F \leq 1)$ shown in Figure 4.5. Therefore, two or more fluids are regarded as a single effective fluid whose properties vary in space based on the F of each phase. If the free surface has the value of $F = 0.5$, which means that a control volume is filled with half of the water and half of the air, respectively.

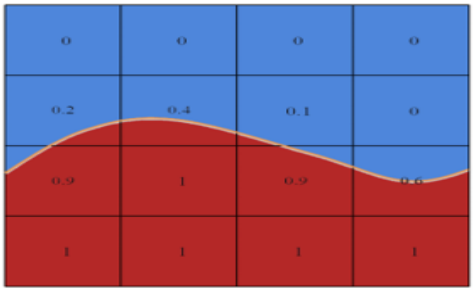

Figure 4.3 Volume of Fluid (VOF) approach (Haider, 2013)

4.8 Wave Forcing Method

It is necessary to run simulations for a long period to investigate physical phenomenon in transient flows around bodies. In Star-CCM+, the wave forcing function enables the user to reduce the computing effort by using reduced-size solution domain in the immediate vicinity of the interest body. It also has an ability to eliminate the problems related to wave reflection at the boundaries. This forcing can be achieved by adding source term in momentum equations and thereafter the solution of discretized Navier-Stokes equations is forced toward another solution (theoretical solution or simplified numerical solution) over a specified forcing zone. Except for the forcing zone, 3-D Navier-Stokes equation is used to solve the fluid flow around the bodies as shown in Figure 4.6.

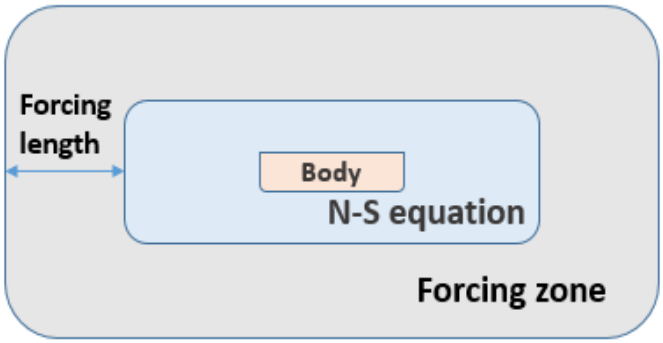

Figure 4.4 Wave forcing region

$$S_{\emptyset}{}' = S_{\emptyset} - \gamma\rho(u_i - u_i{}^*)$$

where $S_{\emptyset}{}'$ is the source term for which forcing is considered, $S_{\emptyset}$ is original source term, γ is forcing coefficient which varies smoothly from 0 at inner edge of the forcing zone to the maximum value at domain boundaries, ρ is the density of fluid, u_i is current velocity and $u_i{}^*$ is the velocity toward which the solution is forced. Instead of velocity u, the forcing source term can be also applied for other physical quantities. The more detailed information can be referred through the user-guide book (CD-Adapco, 2017). Also, this method is based upon Euler Overlay Method that can be referred with specific vertical cylinder problem (Kim et al., 2012).

5 Reference Model

5.1 Introduction

Before proceeding with the present study, it was very important to choose the experiment published previously for a preliminary validation, considering the allowable computing efforts. The test that had investigated wave run-up and air gap response of semi-submersible platform with different values of wave steepness was chosen and had two conditions that consisted of fixed model and moored model under propagating regular waves.

5.2 Reference Model Set-up

The drilling semi-submersible model to be compared with the CFD simulation results was made of wood, steel and plastic and was built with Froude scaling as 1:68 (Figure 5.1). A series of experiments for investigating non-linear wave run-up effects were carried out in the State Key Laboratory of Ocean Engineering basin at Shanghai Jiao Tong University. The basic dimensions of wave basin are 50 m in length, 30 m in breath and 6 m in depth($L \times B \times D$), having different water depths within 4 m. The wave tank is equipped with flap type paddle to generate wave and an absorption wave beach stands at the other side of the basin to eliminate wave reflection. The principle particulars of semi-submersible model are shown in Table 5.1.

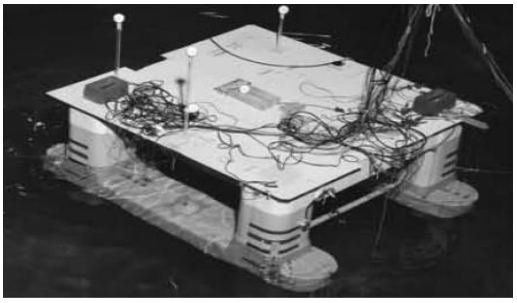

Figure 5.1 Reference experimental model (Shan et al., 2011)

Table 5.1 Main principles of Semi-submersible model (Shan et al., 2011)

	Full scale	Model scale
Draft (m)	17.68	0.26
Column spacing (m)	27.88	0.41
Pontoon length (m)	91.80	1.35
Pontoon width (m)	15.64	0.23
Pontoon height (m)	8.84	0.13
Elevation from base line (m)	31.28	0.46

It should be important to note that the semi-submersible model with these dimensions used for the validation will be mainly used in part 1 of the present studies and be central model for changes in hull displacement in part 2 (Chapter 7), which can be seen later.

5.3 Wave Conditions and Measurements

To begin with, monochromatic regular waves having the two different wave periods were generated with a variety of wave steepness. Table 5.2 shows all wave conditions used in the reference experiment. Even though the wave elevation time histories were actually measured at some locations in the test, specifically, those obtained from two rows of wave probes installed in front of fore and aft columns are of interest for validation with the simulations to be presented later. The schematic layout of the four wave probes located in each row (Row A, B) within one column radius R can be seen in Figure 5.2. The more detailed radial distance from the column wall can be referred in Table 5.3. The initial air gap was kept as 0.197 m during all experiments under fixed condition. The more details of the experiment conditions such as basin, model and waves can be found in reference paper (Shan et al., 2011).

Table 5.2 Regular wave conditions for validation (Shan et al., 2011)

Wave Period T (s)	Wave Steepness (H/L)	Wave Scattering (Ka)
1.0	**1/15**	0.42
	1/20	
	1/30	
	1/40	
	1/50	
1.5	**1/20**	0.19
	1/30	
	1/40	
	1/50	

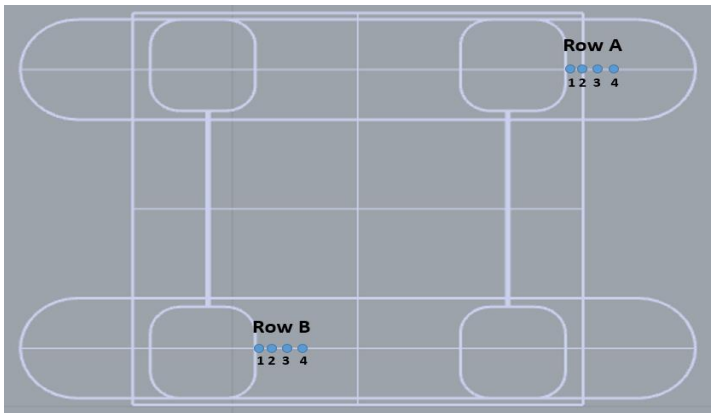

Figure 5.2 Wave probe location on top plan (Shan et al., 2011)

Table 5.3 Radial distance for wave run-up (Shan et al., 2011)

Row	**Point No. 1, 2, 3 and 5 from column wall**
A, B	0.00625R, 0.2R, 0.6R, 1.0R

In order to proceed with the study further, the wave run-up simulation using CFD needs to be validated with experimental data. The steepest waves (Bold at Table 5.2) for each period presented in the reference paper had showed wave run-up time histories which were directly compared with numerically predicted corresponding values.

6 CFD Modelling

6.1 Introduction

This section explains basic computational set-up of this research and specifically focuses on preliminary validations. The Computational domain and boundary conditions for validation cases including the K-Epsilon model for turbulence flow were described in detail. Lastly, in validation study, the comparisons with the results of the simulation demonstrated that wave run-up profile had quite discrepancies with experiment.

6.2 Turbulence Modelling

The K-Epsilon model is chosen to model turbulence, which has been extensively employed in various engineering applications. A major advantage of the K-Epsilon model is that it has relative efficiency about CFU time and physical memory. For example, the Reynolds Stress model usually requires the computation of seven equations in three dimensions, which leads to more efforts while only the two equations are solved in K-Epsilon model. In detail, the realizable K-Epsilon Two-Layer model is applied to obtain stable solutions in fine mesh domain using a two-layer approach since it has more advantages over the standard K-Epsilon model.

A K-Epsilon turbulence model solves transport equations for the turbulent kinetic energy k and its dissipation rate ε. It should be noted that it contains a new transport equation for the turbulent dissipation rate ε and a critical coefficient of the model $(C\mu)$ is expressed as a function of mean flow and turbulence properties. The integral form of transport equations for realizable K-Epsilon model can be shown as follows:

$$\frac{d}{dt}\int_V \rho k\, dV + \int_A \rho k(\boldsymbol{v} - \boldsymbol{v}_g)\cdot da$$

$$= \int_A \left(\mu + \frac{\mu_t}{\sigma_k}\right)\nabla k \cdot da + \int_V \left[f_c G_k + G_b - \rho\left((\varepsilon - \varepsilon_0) + \gamma_M\right) + S_k\right] dV$$

$$\frac{d}{dt}\int_V \rho\varepsilon\, dV + \int_A \rho\varepsilon(\boldsymbol{v} - \boldsymbol{v}_g)\cdot da$$

$$= \int_A \left(\mu + \frac{\mu_t}{\sigma_\varepsilon}\right)\nabla\varepsilon \cdot da + \int_V \left[f_c C_{\varepsilon_1} S_\varepsilon + \frac{\varepsilon}{k}\left(C_{\varepsilon_1} C_{\varepsilon_3} G_b\right) - \frac{\varepsilon}{k + \sqrt{v\varepsilon}} C_{\varepsilon_2}\rho(\varepsilon - \varepsilon_0) + S_\varepsilon\right] dV$$

where:

ρ is the fluid density

k is the turbulent kinetic energy

ε is turbulent dissipation rate

S_k and S_ε are the user-specified source terms

ε_0 is the ambient turbulence value in the source terms that counteracts turbulence decay

f_c is the curvature correction factor

The turbulent viscosity μ_t is computed as:

$$\mu_t = \rho C_\mu \frac{k^2}{\varepsilon}$$

where the coefficient $C\mu$ is the same as value obtained from the boundary layer experiment and no longer constant as with the standard K-Epsilon model:

$$C_\mu = \frac{1}{A_0 + A_S U^* \frac{k}{\varepsilon}}$$

6.3 Computational Domain

The dimension of 3-D computational domain was chosen to accurately simulate non-linear wave run-up phenomenon with efficient CPU times and in order to keep the number of cells within reasonable range. Especially, since there was no specific information about depth in the reference paper, the water depth size (1.8 m) in simulation domain was determined to be large enough for the waves to be considered as deep water waves (Figure 6.1). The numerical tank is largely dimensioned as a length, height and width and in detail there are wave generation zone for Stokes 5th wave and geometric damping zone with gradually increased meshes. The mesh type and quality are significant in accuracy of convergence of the solution as well as computational time.

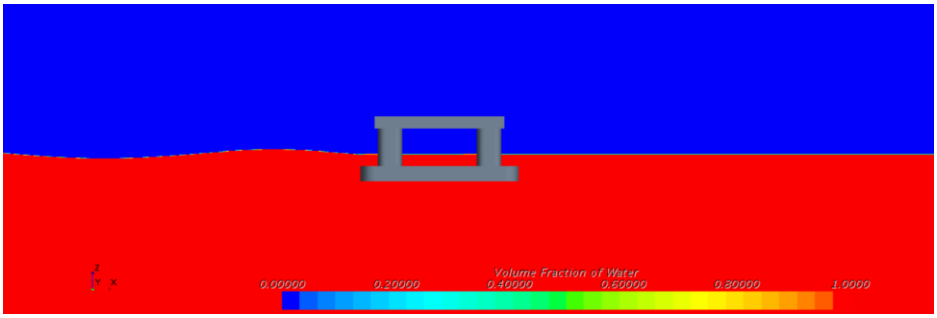

Figure 6.1 Star-CCM+ simulation (t=0s)

In present all CFD simulation, the trimmed mesh was generated in all of the computational domains including regions around semi-submersible model to ensure that the structure of the mesh had both high quality and good anisotropic refinement. With respect to Figure 6.2, the mesh distribution can be seen easily with the detailed domain size (Table 6.1).

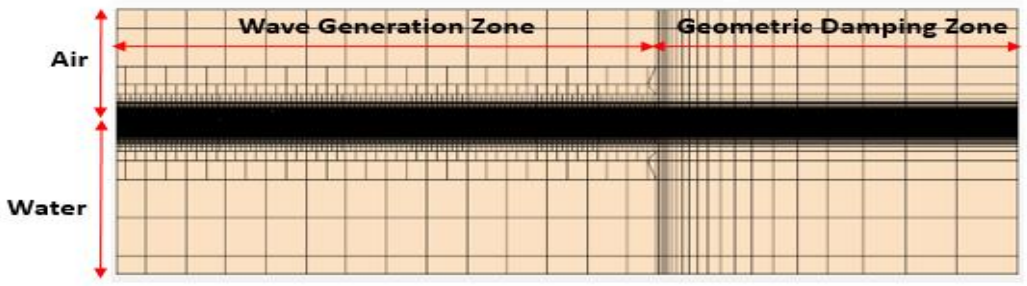

Figure 6.2 Mesh distribution for the validation cases

Table 6.1 Computational domain size for the validation cases

Validation	**T 1.0s** (λ: 1.56m)	**T 1.5s** (λ: 3.51m)
Length (m)	10.10	12.10
Height (m)	Air : 1.35 (L) Water : 1.8 (Deep water)	
Width (m)	2.70 (2L)	
Wave Generation Zone (m)	6.05 (3$L + \lambda + 0.49$)	8.05 (3$L + \lambda + 0.54$)
Geometric Damping Zone (m)	4.05 (3L)	

where L is the total pontoon length and λ is the wave length which is based on linear Airy wave theory. In wave generation zone, marginal lengths such as 0.49, 0.54 m are added for wave forcing function, as will be explained later. The total tank height is 3.15 m including 1.35 m air part and 1.8 m water depth in vertical direction.

The basic coordinate system for the numerical calculation is set as follows: the longitudinal direction of pontoon hull length in x-axis, the vertical direction in z-axis, and lateral direction in y-axis. The pontoon bow of the model is located at the downstream of the inflow boundary about 2 or 4 m (1λ + marginal length) depending on the wave period. In the turbulence flow, the boundary layer flow around the structure wall needs to be approximated using the relevant values such as Reynolds number Re, skin friction coefficient C_f, wall shear stress t_w, and frictional velocity u_f etc. to ensure accurate simulation of the flow field. As a result, the height of the first mesh cell off the wall calculated from flat-plate boundary layer theory is used with an all y+ wall treatment near the wall.

6.4 Release and Ramp Time

Before the release time, any calculation of body motion does not start, which means that some time is needed for initialization. After release time, a ramping function between 0 and 1 is proportionally applied to reduce shock effect caused by sudden changes over a ramp time.

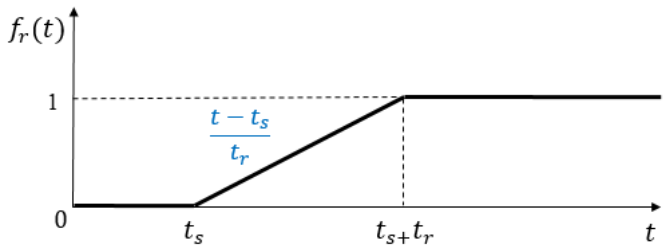

Figure 6.3 The definition of release and ramp time

As presented in the Figure 6.3 above, t_s is the release time, t_r is the ramp time and a different ramping function f_r(t) in each time interval is defined.

Since the simulation begins with the initial fluid configuration of a fully developed wave field, the first wave without diffraction effect normally is ignorable value. The results after the second wave passed the semi-submersible model are therefore considered to perform a reliable analysis. In this regard, it can be said that the ramping function plays a role of controlling the motion by the poor quality wave developed at the beginning.

To summarize, both the diffraction and radiation effect are clearly reflected in the wave run-up results after passing through the time $(t_s + t_r)$. The details on this function can be referred to (CD-Adapco, 2017).

6.5 Boundary Conditions

The initial and boundary conditions must be specified to compute calculation in CFD simulations. Firstly, the wave initial condition was set to a completely developed velocity field away from one wave length (λ) from inlet boundary. The Stokes 5th order wave approximation was used to specify the velocity. This wave is introduced into the domain at the inlet boundary through the velocity inlet boundary condition and extracted from the domain at the outlet boundary through the pressure outlet boundary condition. Both the top and both side boundaries are set as symmetry plane boundary condition (shear stress is zero) and no-slip wall boundary condition (normal velocity is zero) is applied at the surface wall of the semi-submersible structure. In this simulation, it should be noted that the velocity inlet boundary condition is set at the bottom of the computational domain. Figure 6.4 describes numerical tank implemented with all the boundary conditions.

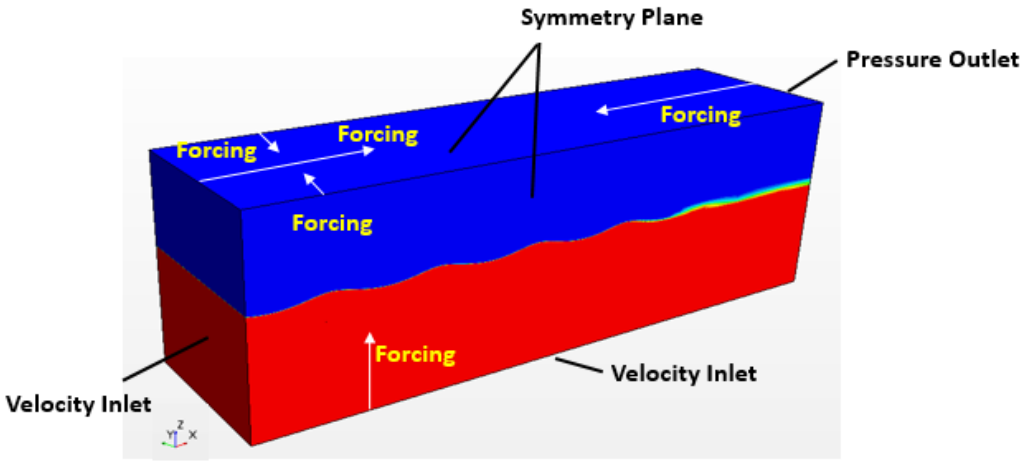

Figure 6.4 Boundary conditions

Forcing length is defined as a distance from the boundary at which the forcing starts. The specified value must be at least one wavelength and the forcing zone cannot also start close to the body of interest (CD-Adapco, 2017). Both the wave forcing from the outlet boundary and geometric damping zone are used to dissipate the energy by the wave and minimize the reflection of the wave. Through the numerous parametric studies on forcing length, the most

appropriate values at each boundary were found and expressed as a multiple of the known parameters presented in Table 6.2.

Table 6.2 Forcing length at each boundary for validation cases

Boundary condition	T 1.0s	T 1.5s
Inlet	1.56 (λ) m	3.51 (λ) m
Outlet	3L (4.05 m)	
Bottom	$\frac{2}{3}d$ (1.20 m)	
Sides	$\frac{1}{3}L$ (0.45 m)	
Top	-	

where λ is wave length based on linear Airy theory, L is the total pontoon length and d is water depth of the computational domain in order to allow for deep water condition.

6.6 Validation Study

6.6.1 Introduction

For the sake of validation of CFD numerical simulation, wave run-up profiles along the platform columns were compared with model test data. The free surface elevations in front of fore and aft columns in the fixed condition were specifically monitored by numerical wave probes where the experimental wave probes were placed, and confronted with the experimental data for the steepest wave in each period (T1.0s and T1.5s at the model scale). As a result, this validation work seems to have quite reasonably similar trends except for crest and trough in the time series of wave run-up while comparison of wave elevation showed good agreements.

6.6.2 Wave Elevation

A series of convergence studies for incoming waves were conducted to determine the mesh size and time step as shown in Figure 6.5. The coarse mesh in free surface region has a possibility of making breaking wave or dissipation while the very fine mesh can be time-consuming. Thus, the mesh sizes in the horizontal and vertical directions were varied to find where the wave height converges with various time steps.

The Courant number (CFL) is defined as $\frac{U\Delta t}{\Delta x}$ and generally calculated for each cell. If this number is less than or equal to 1, the numerical simulations can be considered as stable, leading to converged solutions. Therefore, it is essential to consider the CFL number when determining the mesh size and time step. In wave generation, it is appropriate to express mesh size and time step as a fraction of wave properties. Finally, the number of mesh was chosen as one hundredths of the wave length, one fortieth of the wave height, and the time step size was one thousandth of the wave period in each wave condition as summarized in Table 6.3.

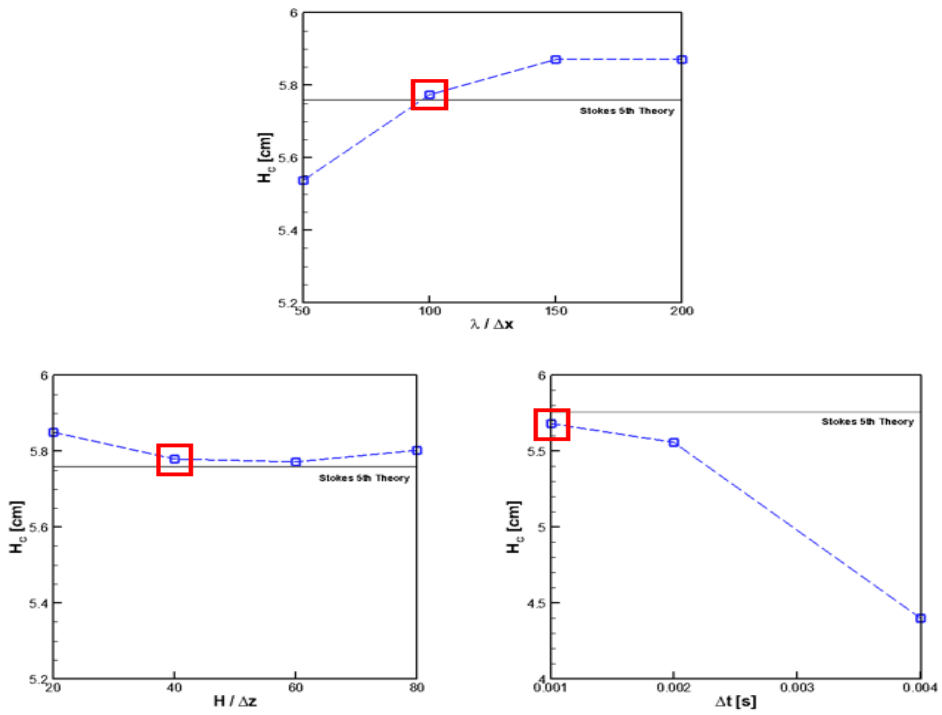

Figure 6.5 Mesh convergence test for validation cases

Table 6.3 Mesh size in the wave generation region for validation cases

Δx	$\lambda/100$
Δz	$H/40$
Δt	$T/1000$

A linear wave theory referred as Airy wave theory is often applied to get a quick and rough estimate of wave characteristics and effects. On the other hand, a Stokes wave is a non-linear and periodic surface wave obtained using perturbation series expansion. This theory has been usually applied to intermediate and deep water conditions, which means that the ratio of the water depth to wave length is over at least 0.05.

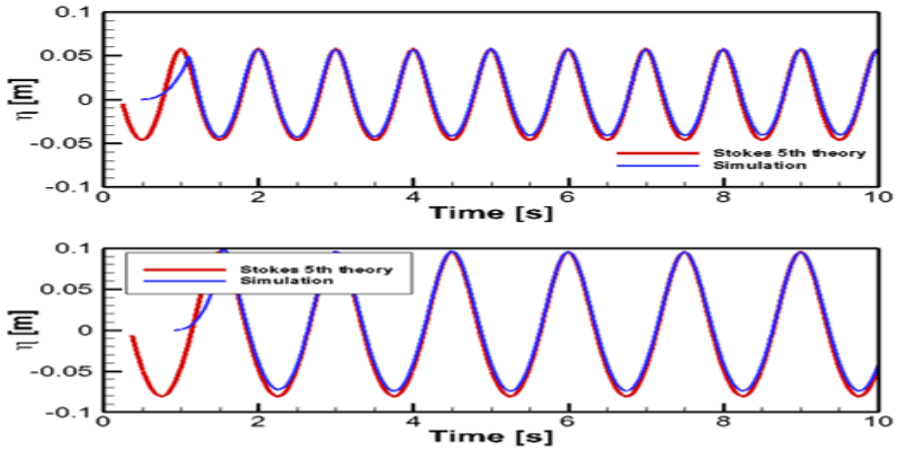

Figure 6.6 Wave validations

When compared with the linear wave that has sinusoidal-shape, the surface wave profile of stokes wave has relatively sharp crests and even troughs. Therefore, it represents wave non-linear effect clearly and also tends to be closer to the real ocean wave as the order of Stokes wave increases. In CFD calculations here, the Stokes 5th waves were simulated and monitored for the locations of x = 2 or 4 m (1.0s, 1.5s each) where the pontoon bow of the semi-submersible model will be placed later. Then, these numerical results were validated with analytical solutions of the corresponding theory against wave elevation to examine the accuracy of the CFD wave generation on the computational domain. The

comparisons of wave elevation time history for only the steepest waves for each period are illustrated in Figure 6.6. As can be seen from this result, there are few discrepancies in the wave crest, whereas wave trough showed up to about 10.0 % between present simulations and analytical solutions.

6.6.3 Wave Run-up

A comparisons of the wave run-up elevation were performed as means for validating numerical method (CFD) to be used further. The wave run-up simulations around fore and aft columns of semi-submersible in fixed condition are presented as shown by Figure 6.7 and Figure 6.8 with time period 1.0s, 1.5s, respectively.

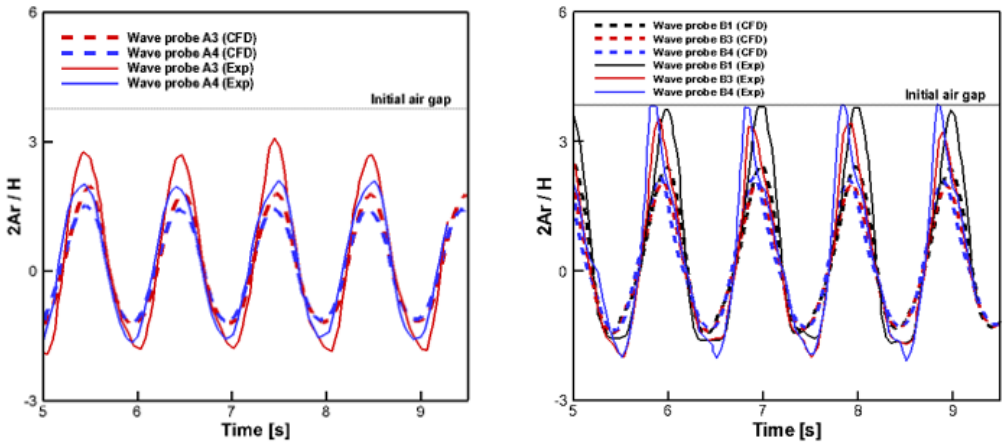

Figure 6.7 Wave run-up. Experimental and Numerical (T1.0s, L: Fore, R: Aft col)

In the graphs, the solid line represents the experimental data from reference and the dotted line shows the simulated values obtained from Star-CCM+ in this study. The left side on each figure is normalized wave run-up elevation around fore column and the right side is for aft column. (Ar is the local wave elevation, H is undisturbed incident wave height)

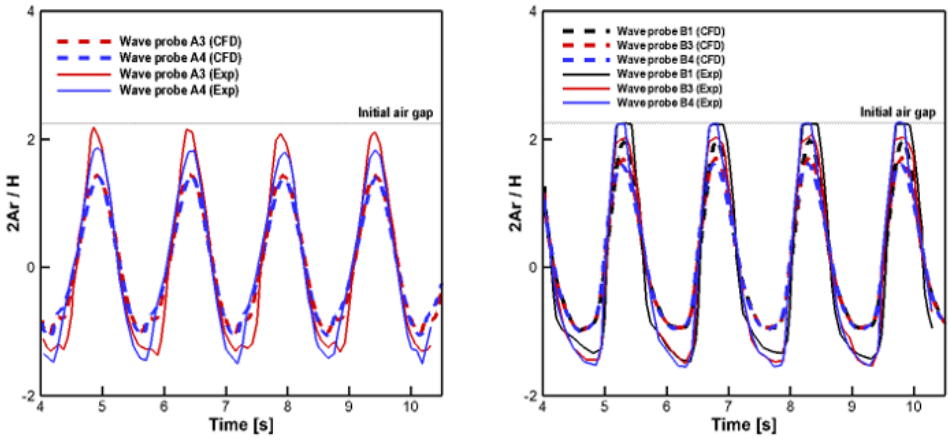

Figure 6.8 Wave run-up. Experimental and Numerical (T1.5s, L: Fore, R: Aft col)

As expected, wave steepness related to wave period appeared to have an effect on wave run-up profile shape and specifically wave run-up comparisons around aft column in the wake zone of fore column showed the somewhat large discrepancies near maximum crest due to non-linearity and strongly wave – column interaction, specifically for relatively shorter wave (Figure 6.7). Therefore, it is found that the simulation of the wave run-up with short wave period (steep-wave) requires more careful attention to the areas where the interference under deck and around columns takes place for capturing the accurate run-up behaviours clearly, especially for aft columns. From these validation results with experiment, monitoring wave run-up elevation positioned within one radius of column is demanding task, which means that there should be some differences between experiment and numerical method without extremely fine mesh.

7 Hydrodynamic Set-up (Linear analysis)

The same semi-submersible model used in the CFD simulation of the part 1 was modelled by the panel method using GeniE based upon the finite element method (FEM). The submerged hull surface had to be panelled except for water surface so that boundary element method (BEM) can be used to solve this boundary value problem (BVP). The only first-order velocity potential was solved using Wadam to obtain the theoretical prediction of wave run-up RAOs at the specified locations. In other words, Wadam itself calculates the wave elevation per incident wave amplitude from the specified positions when the model is fixed. In this study, these values were used as results of the wave run-up calculation for direct comparisons with CFD results. As presented in Figure 7.1, it shows the panel model to be used in the hydrodynamic analysis.

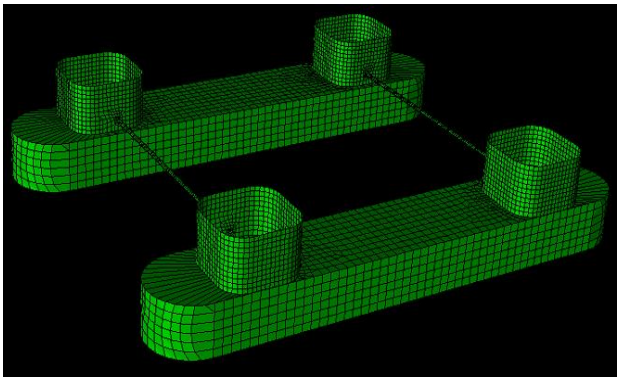

Figure 7.1 Hydrodynamic panel model for part 1

For a semi-submersible modelled as panels, the panels of different sizes were set to each part of the model corresponding to the relative importance about the phenomenon. At first, the panel sensitivity test for efficient CPU times was performed in a similar manner to mesh convergence test of the CFD simulation conducted previously. At a wave probe location, the wave run-up RAOs with varying the number of panels were plotted for comparisons to find the most appropriate converging point. In general, potential theory does not have obvious sensitivity to panel number. This can be easily seen from Figure 7.2 that there was no significant difference depending on the number of panels. However,

among five sets of panels tested here, the wave RAOs in about 7100 panels tended to converge when compared to those of other panels. Therefore, unless explicitly stated otherwise, a hydrodynamic model of the panel (n=7102) assumed to be converged would be consistently adopted for computations.

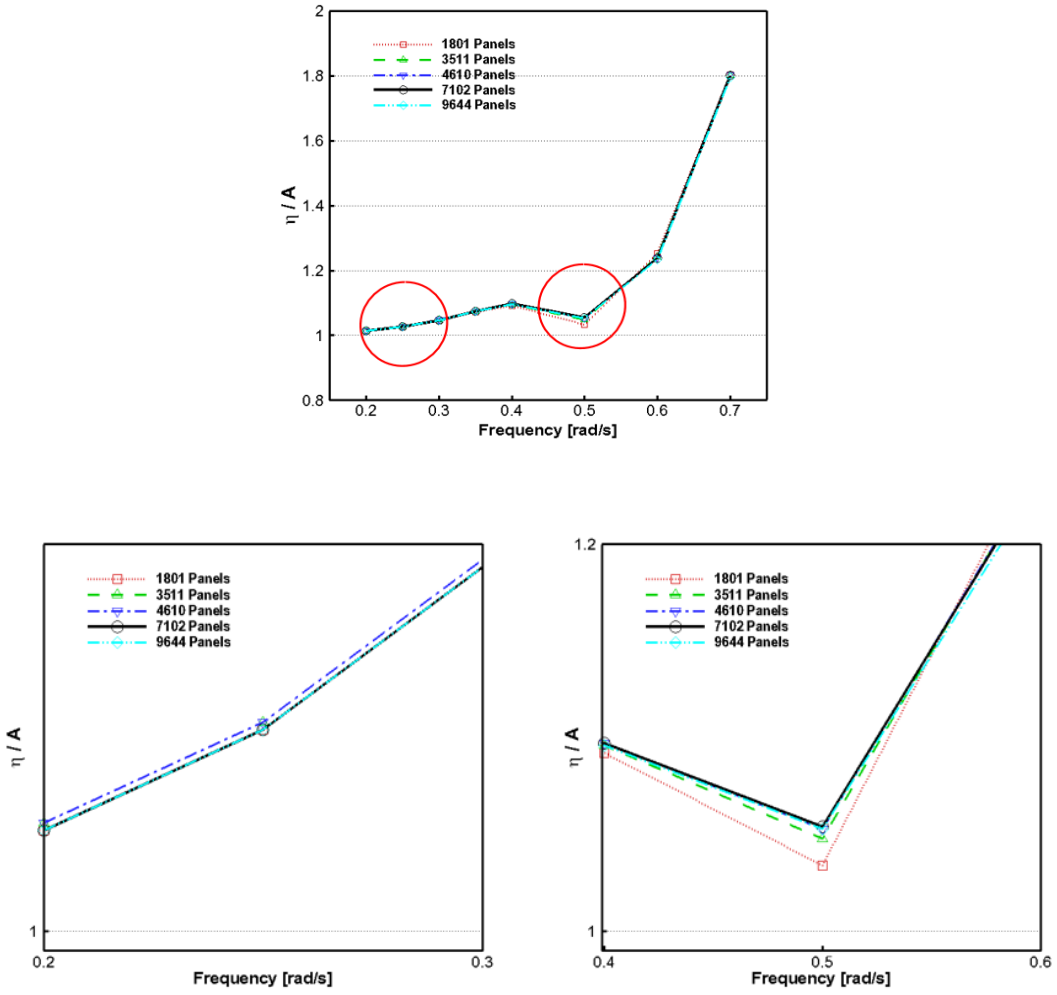

Figure 7.2 Panel convergence test

The FEM file exported from GeniE was directly imported into the Wadam. As aforementioned, this software is based on linear Airy theory and potential flow theory and makes it possible to gain results in a form as complex transfer function. It has been employed to consider wave including incident and diffracted based on a prototype model (full scale) unlike the CFD simulations on a scaled basis ($\lambda = 68$). The detailed setting values for the numerical result are presented in Table 7.1.

Table 7.1 Setting for linear diffraction analysis for part 1

Wave direction	180 deg (head sea)
Frequency set	0.2, 0.25, 0.3, 0.35, 0.4, 0.5, 0.6, 0.7 rad/s
Draft	0.26 m
Radius of gyration (R_{xx}, R_{yy})	0.41 m, 0.43 m (at COG)
Centre of gravity (x, y, z)	0.68 m, 0 m, 0.33 m (from base line)
Total mass	103 kg

8 Parametric Studies

8.1 Introduction

As a part 1 of the present studies, wave run-up phenomenon was investigated depending on different wave frequencies and steepness for heading regular waves using Star-CCM+ (fully nonlinear) and Wadam (1st order diffraction analysis). The same semi-submersible model previously used for validation cases was employed, but some CFD computational set-ups were slightly changed to simulate new wave condition set with reference to ITTC (2011b) recommendations due to the long period wave. On the other hand, in part 2, the analysis of the wave run-up was performed based on the volume displacement of the model, the main parameter, under an identical regular wave condition with different wave frequencies for a wave height. The hull displacement was varied to be half and double part 1 basic model and thereafter a displacement model having the most remarkable wave run-up values among them was chosen to examine the draft effect by adding the survival conditions with existing operational condition.

8.2 Part 1

8.2.1 Model and Wave Conditions

A brief description of the part 1 in current studies was that systematic investigation on wave run-up phenomenon was carried out by using Star-CCM+ and Wadam. In other words, fully nonlinear numerical model (CFD) has been computed and compared with numerical panel model established by use of Wadam. From this study, not only validity of linear numerical free surface wave modelling can be observed but also non-linearity associated with the wave higher order component on the wave run-up around columns are presented.

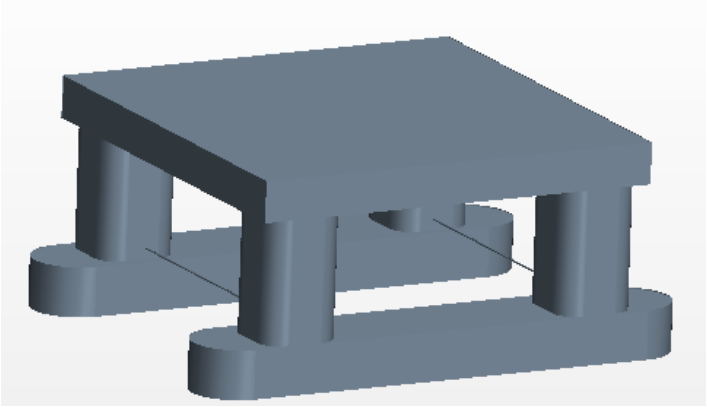

Figure 8.1 The same computational model as previous validation cases

The same model which had been used in validation cases described earlier was employed for part 1 simulations (Figure 8.1). The detailed information about the semi-submersible model can be referred in Chapter 3. A set of regular waves with three different wave height depending on the wave frequency ranging from 0.2 to 0.7 rad/s (at full scale, $\lambda = 68$) were shown in Table 8.1. The wave steepness as one of the significant parameters was varied from 0.0022 until 0.0811.

Table 8.1 Regular wave conditions for part 1

Wave height H (m)	Wave frequency ω (rad/s)	Wave length λ (m)	Wave steepness S
0.05 0.10 0.15	1.65	22.66	0.0022 – 0.0811
	2.06	14.50	
	2.47	10.07	
	2.89	7.40	
	3.30	5.67	
	4.12	3.63	
	4.95	2.52	
	5.77	1.85	

8.2.2 Computational Set-up

Detailed explanations to consider when determining the computational domain size have already been discussed before in Chapter 4. However, the method for the size of the numerical wave tank (NWT) used for the validation shown in the Table 6.1 will no longer be used since a wave with a relatively long period can be easily influenced by the wave reflection from outlet boundary. Thus, convergence studies (length, width) for the NWT were conducted through several trials and errors, considering the wave period to be a three-dimensional domain. It should be also noticed that the water depth in the domain was set to be half of each wave length for deep water condition while the air region remained constant (1.35 m) regardless of the wave condition. Information on the size of the NWT is summarized (Table 8.2) and illustrated with mesh distribution (Figure 8.2).

Table 8.2 Computational domain size

Wave Generation Zone (m)	$2.5\lambda + L + 0.5$
Damping Zone (m)	1.5λ

Length (m)	$4\lambda + L + 0.5$
Height (m)	Air : 1.35 (L) Water : 0.5λ (Deep water)
Width (m)	6.75 ($5L$)

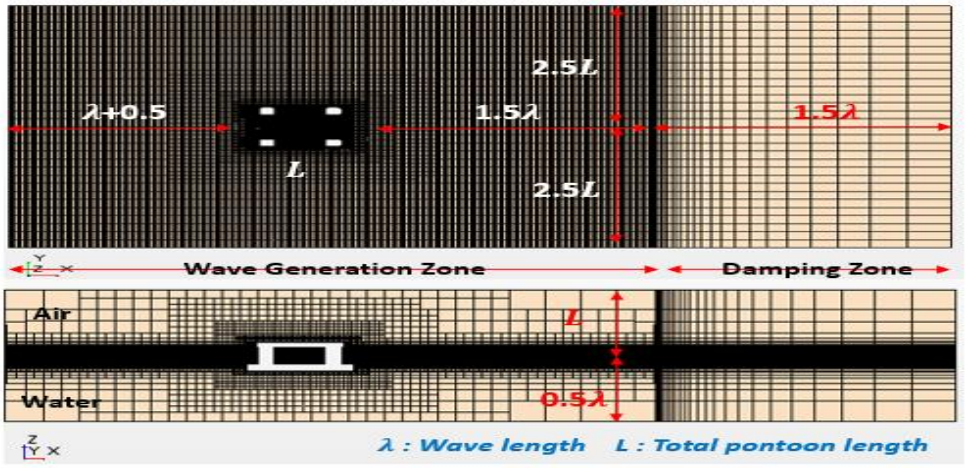

Figure 8.2 Mesh distribution (top view and side view)

With respect to the wave generation, since the waves with long period must be simulated with small errors by reflection, the results of convergence tests of the relevant parameters (Table 6.3), which were performed earlier, were found to be have too many meshes. Therefore, according to the guidelines for ship CFD applications from ITTC (2011b) recommendations (a minimum of 80 cells per wave length, 20 cells of wave height), the mesh size and time step were modified reasonably and also applied to the wave run-up simulation with model. The mesh size in vertical and horizontal directions on free surface region could be refined with time step related to wave period as below (Table 8.3). With this, the Stokes 5th order wave was used and its wave elevation was found to be sufficiently acceptable for the current mesh size and time step compared to the theoretical one, which showed approximately the same order of discrepancy as seen in previous wave validation results (Figure 6.6).

Table 8.3 Mesh size in the wave generation region

Δx	$\lambda/100$

Δz	$H/20$
Δt	$T/512$

The initial and boundary conditions are the same as those used for validation cases. To summarize, the simulations were started with a fully developed wave field with a distance one wave length in advance. The inlet and bottom of the domain were set as velocity inlet and outlet was set as pressure outlet boundary condition. The symmetry plane boundary condition was applied to the top and sides while the structure model was set as no-slip wall condition. The forcing method is essential to reduce the computational time effectively, especially for 3-dimentional tank used in here. Therefore, setting for the forcing length at each boundary can be an extremely important procedure at early set-up stage for computation, where the method for determining the proper length based on each wave condition is similar to that described in Table 6.2. The generalized forcing lengths using the wave properties are as follows (Table 8.4).

Table 8.4 Forcing length at each boundary

Boundary condition	Forcing length
Inlet	$\boldsymbol{\lambda}$
Outlet	$\boldsymbol{1.5\lambda}$
Bottom	$\frac{2}{3}\boldsymbol{d} = \frac{1}{3}\boldsymbol{\lambda}$
Sides	$\frac{5}{6}\boldsymbol{L}$
Top	-

where λ is the wave length based on linear Airy theory, L is the total pontoon length and d is water depth of the numerical wave tank (NWT) so as to make wave region be deep water condition.

8.2.3 Results and Analysis

In order to verify the effect of wave steepness on the wave run-up through both the linear and nonlinear analysis, the part 1 of the present studies was performed with the semi-submersible model used in validation cases before.

In this section, the predicted results of the numerical simulation are compared with the results based on potential flow theory, indicating that the results had similar variation tendency in graphs, and even captured detailed areas where non-dimensional run-up was declined. Figure 8.3, 8.4 present the maximum wave elevations around the column, which have been normalized by the undisturbed wave crest height (non-dimensional wave run-up) depending on the wave frequency in x axis. Here, the wave crest height means incident wave amplitude that can be defined as the half of wave height for the linear wave. To calculate these values in CFD simulation, after at least the second wave passes, maximum wave elevations over the five periods were considered to obtain the representative mean (r) for each condition which would be used for the following comparisons in y axis.

As shown by following eight graphs, in both columns, a comparison between the numerical values with difference values of wave height and theoretical ones commonly demonstrated large discrepancies in the range of 0.4 rad/s to 0.7 rad/s. In these higher wave frequencies, the numerical results in the aft column (B) were also found to generally have larger scatter than corresponding one (A). According to 1^{st} order flow calculations, it showed that wave run-up values were somewhat lower than those predicted numerically which is based on Stokes 5^{th} wave theory. These are attributed to the fact that aft column is exactly in the wake region of the fore column, which means that rear area has relatively complex wave nonlinear characteristics. In other words, the strong influence of nonlinear diffraction effect related to higher wave component can be thought to be dominant around aft column of this type of platform.

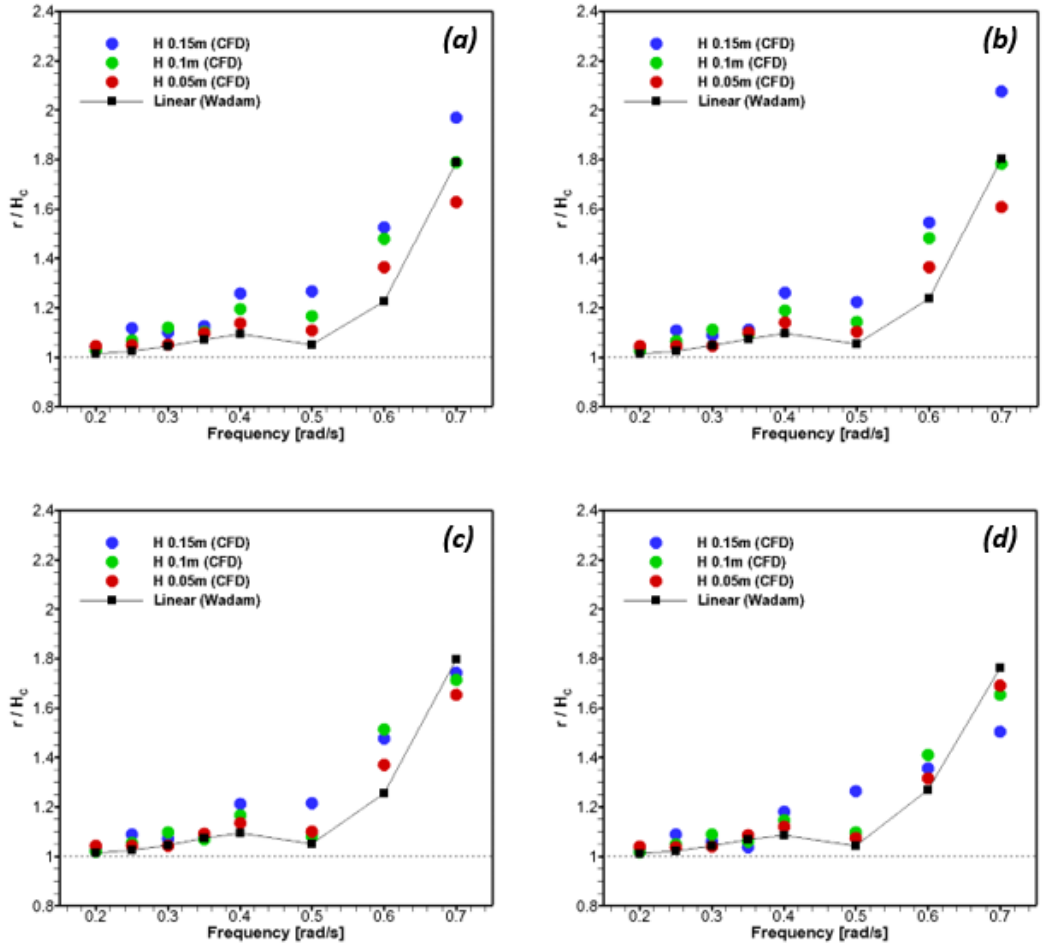

Figure 8.3 Non-dimensional wave run-up depending on wave height in fore column (A) (a) A1, (b) A2, (c) A3, (d) A4

However, it should be noticed that at the highest frequency of 0.7 rad/s, the numerical values seemed sometimes to be lower rather than the linear values; especially for low wave height. One reason for this may be probably that an incident wave with a high frequency approaching the column tends to be broken more easily by reflected waves and diffracted waves than the others, which means that it has a chance to interact more frequently among the nonlinear waves. Therefore, these nonlinear interactions can rather result in a small run-up value with offset effect.

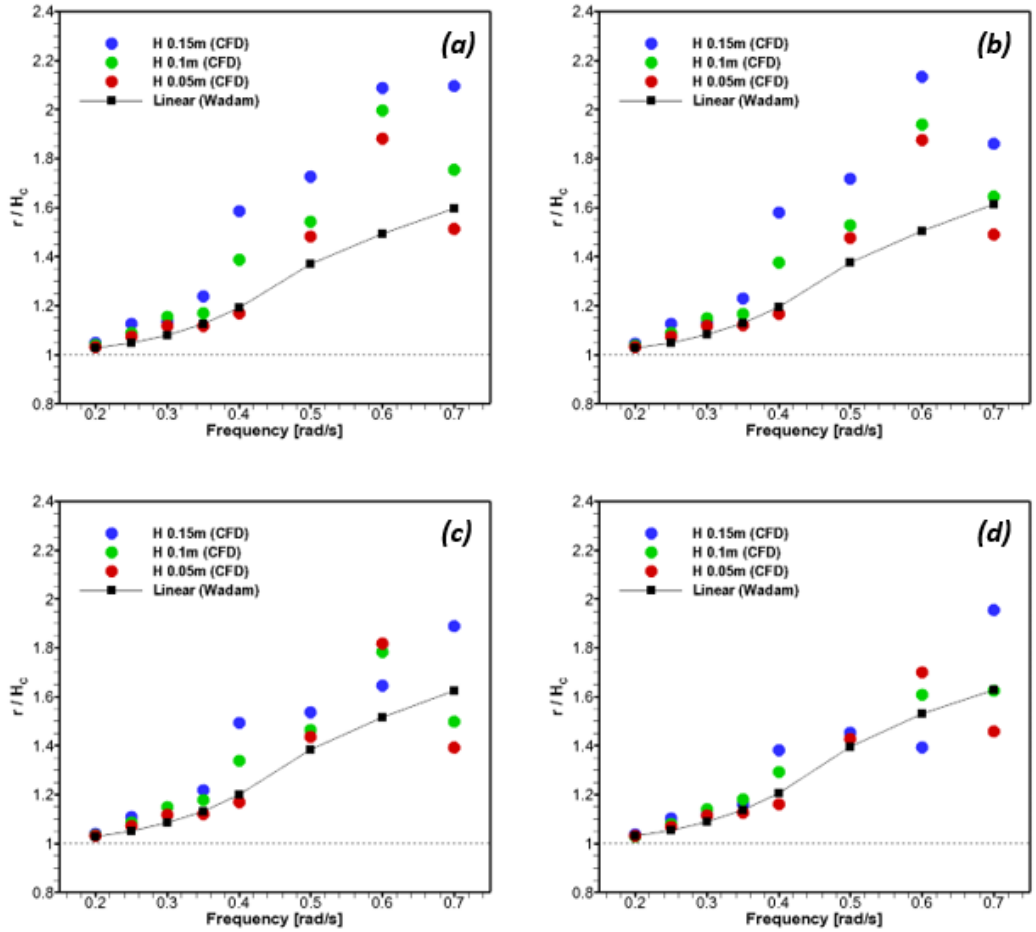

Figure 8.4 Non-dimensional wave run-up depending on wave height in aft column (B) (a) B1, (b) B2, (c) B3, (d) B4

Firstly, the non-dimensional wave run-up was basically varied depending on the WP location. As expected, results from standard linear analysis appeared to be almost identical around each column since locations of the respective monitoring probes are very close within one radius. Secondly, it is interesting to observe that CFD run-up heights were increased by a factor of up to 2.1, which occurred at the second nearest probe (A2, B2) in front of each column for wave height 0.15 m. This is because the wave diffraction was intensified in the location that is not the closest rather. In addition, the wave reflected against the column wall might also play an important role in causing significant wave run-up with superposition of incident wave, which is the similar principle as wave jetting occurrence under deck. From the comparison of results, linear analysis may underestimate

maximum wave elevation, specifically in the region close to columns due to run-up effects when it was compared with CFD computations based on fully nonlinear analysis.

Some simulation snapshots for visualization of process in CFD are illustrated in Figure 8.5, showing the wave run-up phenomenon close to each column clearly with qualitative aspects. With respect to this figure, left side (a, c) showed the maximum run-up on the fore column and the other side (b, d) is about after column from 2D and 3D views.

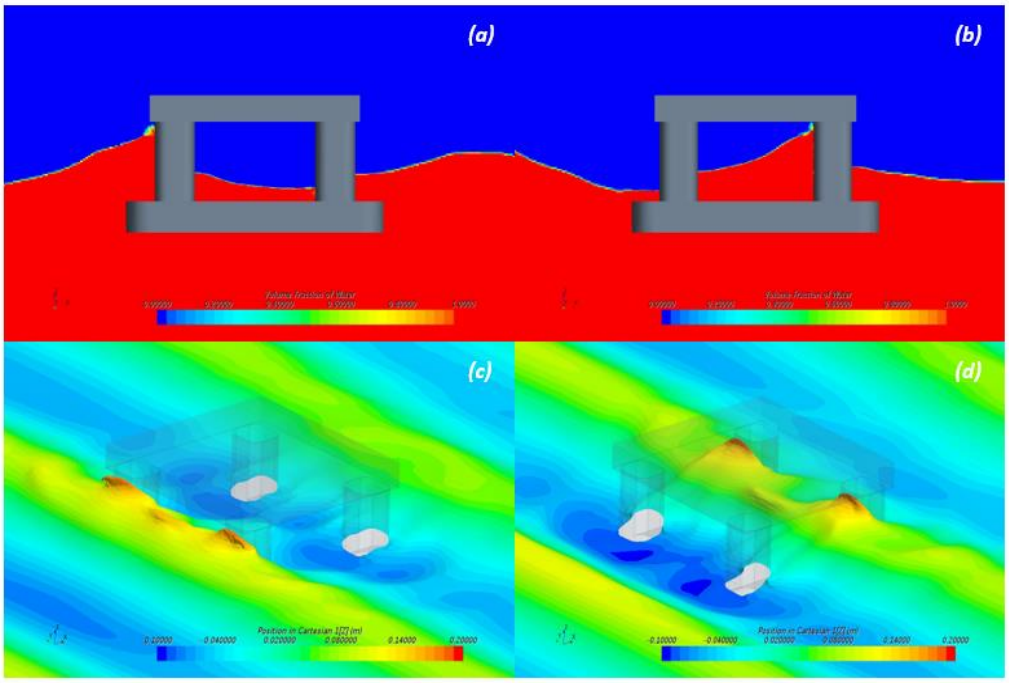

Figure 8.5 Wave run-up simulation snapshots in the steepest wave (T 1.09s, H 0.15m)

In order to investigate the effect of the wave steepness along the distance from the column wall, six graphs in the Figure 8.7 were plotted for each column as follows. Similar to the definition of the previous graph, maximum wave elevation normalized by incident(undisturbed) wave crest height was plotted with the horizontal axis normalized by column radius R where a, b denoted the distance from each column wall (A, B) within one radius, respectively.

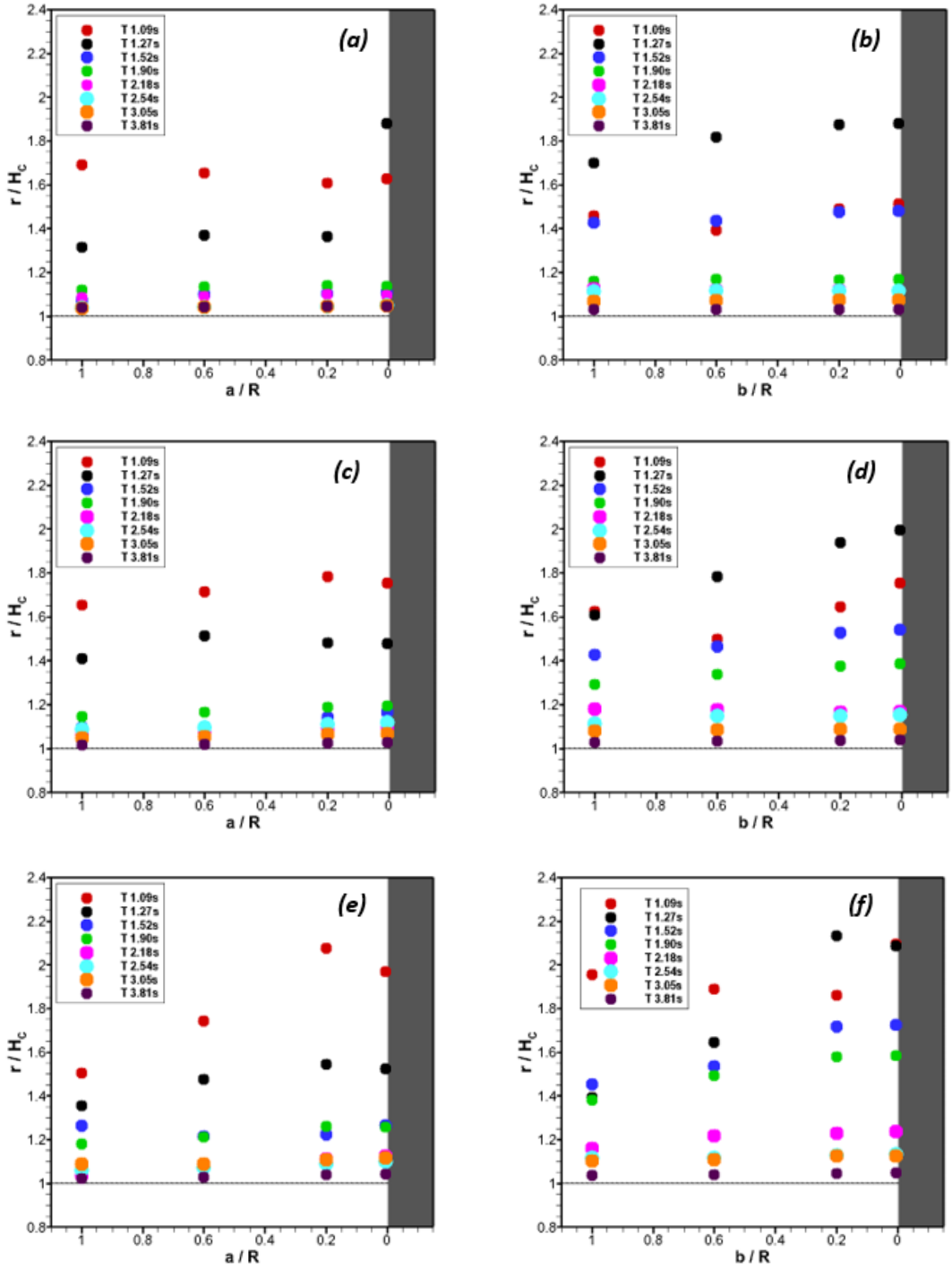

Figure 8.6 Non-dimensional wave run-up along the distance from the column (a), (b) H 0.05m; (c), (d) H 0.10m; (e), (f) H 0.15m

In fore column (A), maximum wave elevation tended to remarkably increase with the wave steepness over 2.0 %, showing at least approximately 1.2 up to 2.1 higher than the incident wave amplitude. Also, most of these values along the

distance from column showed roughly the similar magnitude except for the highest wave height (e). The conditions where the wave steepness is less than 2.0 % have shown that there is no significant difference by both wave steepness related to wave period and distance from the column. On the other hand, in aft column (B), when the non-dimensional wave run-up values are compared to those obtained in fore column, it obviously suggested that the values were much more sensitive to the wave steepness due to nonlinear effects related to second and higher-order wave interaction with columns including underwater pontoon. Furthermore, from presented in Figure 8.6 (b, d, f), the closer it is to wall, the higher wave run-up is, which means that the extent of the run-up in front of aft column is dependent on the distance from the wall. The maximum wave elevations were found to be 1.4 to 2.1 times as high as the magnitude of the incident wave amplitude for steepness over 2.65 % (d, f).

8.3 Part 2

8.3.1 Models with different displacements

As part 2 of the current studies, wave run-up phenomenon was investigated with different size models, indicating that hull volume displacement was varied with constant ratio based on the model used in part 1, shown in Table 8.5. Instead, the regular wave condition was considered for the only one wave height, which was 0.10 m in part 1 so as to purely understand the effects associated with the hull size. It can be easily seen in Table 8.6. For this work, the simulations using Star-CCM+ were run and compared in terms of particulars of the model. And then, draft conditions as one of the main variables were added to see how much this directly influences on wave run-up height and these numerical results were analysed deeply.

Table 8.5 Model dimensions with different volume displacements

Model	Down	Original	Up
Draft (m)	0.206	0.260	0.328
Pontoon length (m)	1.071	1.350	1.701
Pontoon width (m)	0.183	0.230	0.290
Elevation from base (m)	0.365	0.460	0.580
Column diameter (m)	0.167	0.210	0.265
Air gap (m)	0.159	0.200	0.252
Volume displacement (m^3)	0.05125	0.10249	0.20499

As can be observed in Table 8.5, the volume displacement was changed to make it half and double with reference to original model's one. Thereafter, other main dimensions were naturally varied according to the ratio between them. In the case of volume, it is simply proportional to the cube of the length ratio as known.

Table 8.6 Wave conditions for part 2

Wave height H (m)	Wave frequency ω (rad/s)
0.10 m	1.65, 2.06, 2.47, 2.89, 3.30, 4.12, 4.95, 5.77

In the computational set up, the numerical wave tank (NWT) has been determined by using both pontoon length (L) and wave length (λ), which can be referred in Table 8.2. Thus, on CFD simulations in part 2, the sizes of the computational domain were calculated according to the values of each model and wave condition, and the wave forcing length at the boundaries was also obtained as the method specified in Table 8.4. Generating regular waves has already been done earlier and therefore left out here, because one (0.10 m) of the three wave heights used in part 1 was representatively selected for part 2. Further information on these simulation settings can be found in chapter 8.2, in more detail.

8.3.2 Results and Analysis

Figure 8.7, 8.8 show maximum wave elevations around each column within one radius with varying hull volume displacement. The 'Down' denotes a model that has half the original model volume while 'Up' refers to a model with double quantity. It should be kept in mind that the wave heights used here are same.

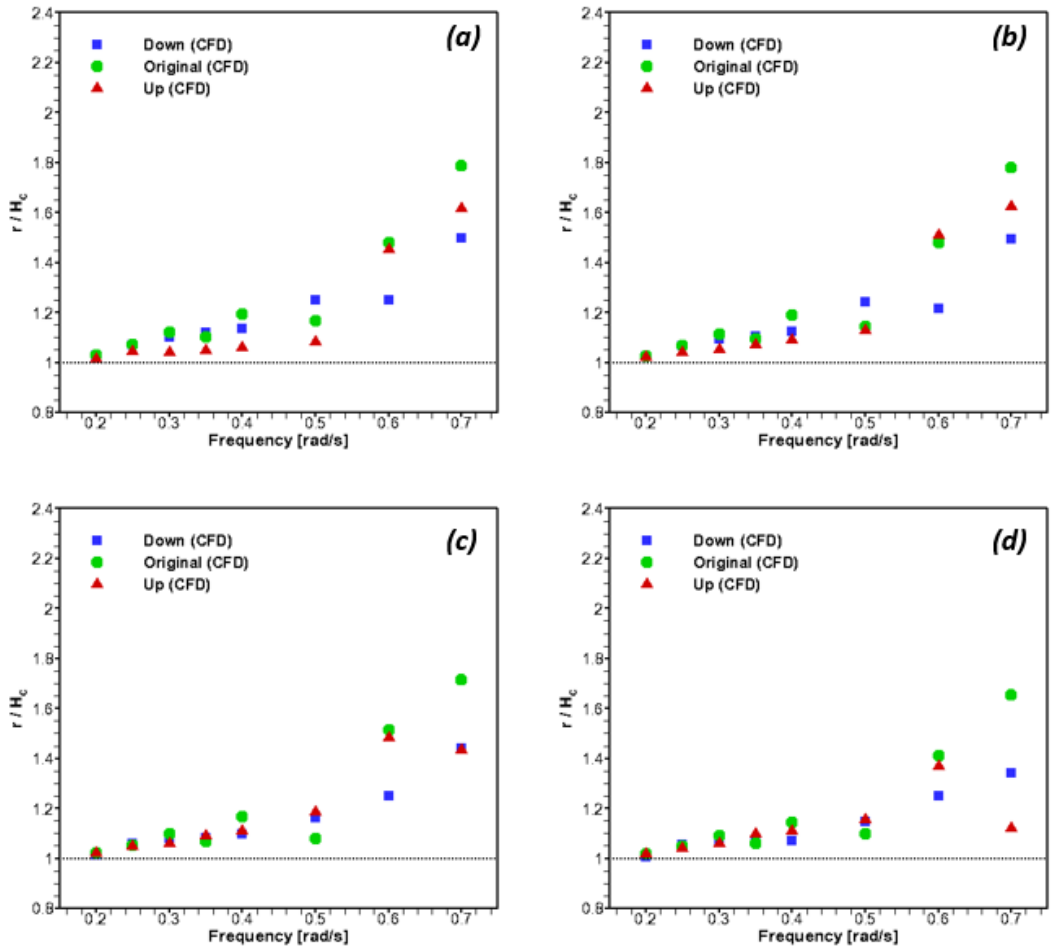

Figure 8.7 Non-dimensional wave run-up depending on volume displacement in fore column (A) (a) A1, (b) A2, (c) A3, (d) A4

Firstly, in the fore column (A), it can be easily seen in the Figure 8.7 that the magnitude of wave run-up height depending on model displacement is slightly different in the case of A1, A2 close to the column, whereas it is almost similar in the case of A3, A4 for the wave frequency less than 0.4 rad/s. In the wave over 0.4 rad/s, most of the large values for each wave frequency are shown in 'original'

model. It might be due to that the wave is relatively less likely to be affected in 'down' model, and column of 'up' model played a role in generating reflected wave as barrier, causing wave run-up reductions to some extent. At the highest frequency of 0.7 rad/s in 'original' model, maximum wave run-ups of about 1.8 times as incident wave amplitude are evenly observed from A1 to A4.

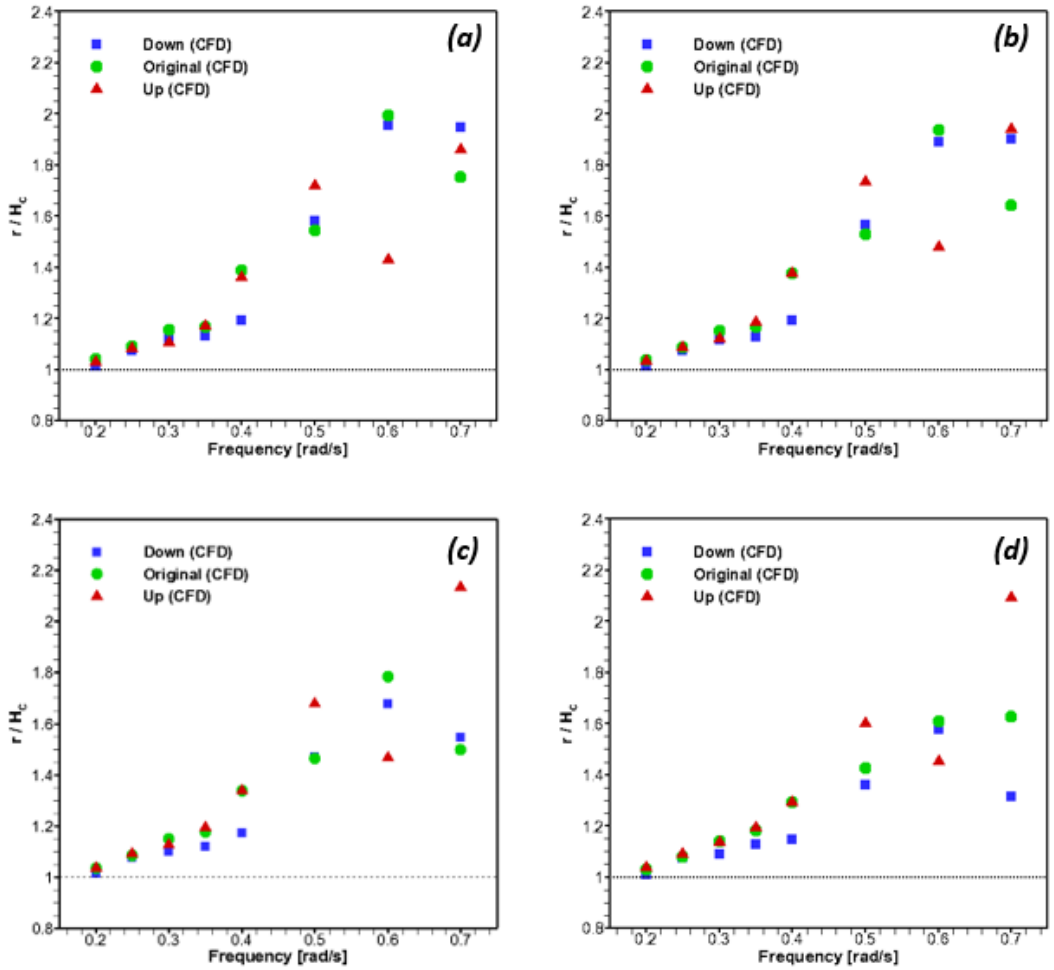

Figure 8.8 Non-dimensional wave run-up depending on volume displacement in aft column (B) (a) B1, (b) B2, (c) B3, (d) B4

Secondly, in the aft column (B), the magnitude of the wave run-up with three displacements shows trivial differences for the wave frequency less than 0.4 rad/s, as presented in Figure 8.8. However, it can be seen that the influence of the wave run-up effects is critical in waves with relatively short period (wave frequency of 0.4 or more), especially in the 'up' model where the displacement is

large. Specifically, maximum values show roughly up to 2.2 higher than the incident wave amplitude at 0.7 rad/s when the wave period is the smallest but these were monitored at B3, B4 rather than near the column. Due to the large column diameter, it can be thought that the value was remarkably decreased at B1, B2. Overall, there is also a large scattering in the aft column when compared with the other.

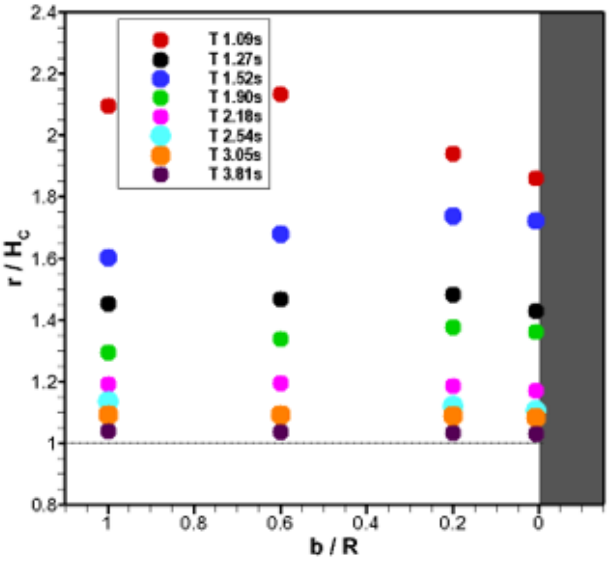

Figure 8.9 Non-dimensional wave run-up along the distance from the aft column (B) ('Up' model)

Figure 8.9 represents at a glance what has been described above where b denoted the distance from the aft column wall (B) within one radius in x axis. In the other displacement conditions, the wave run-up values along the distance from each column had a similar pattern to those of the condition with different wave height as presented in Figure 8.6. In conclusion, it can be deduced from this aspect that in the model with large volume displacement, there will be a significant run-up increase in the locations that are not near the aft column.

Figure 8.10, 8.11 shows statistical regression analysis of the wave run-up based on the ratio of the column diameter to the wave length by employing linear least square method. The x-axis in the graphs represents the ratio of column diameter

(D) to the wave length (λ), and the y-axis is the wave run-up value relative to the incident wave amplitude as calculated so far.

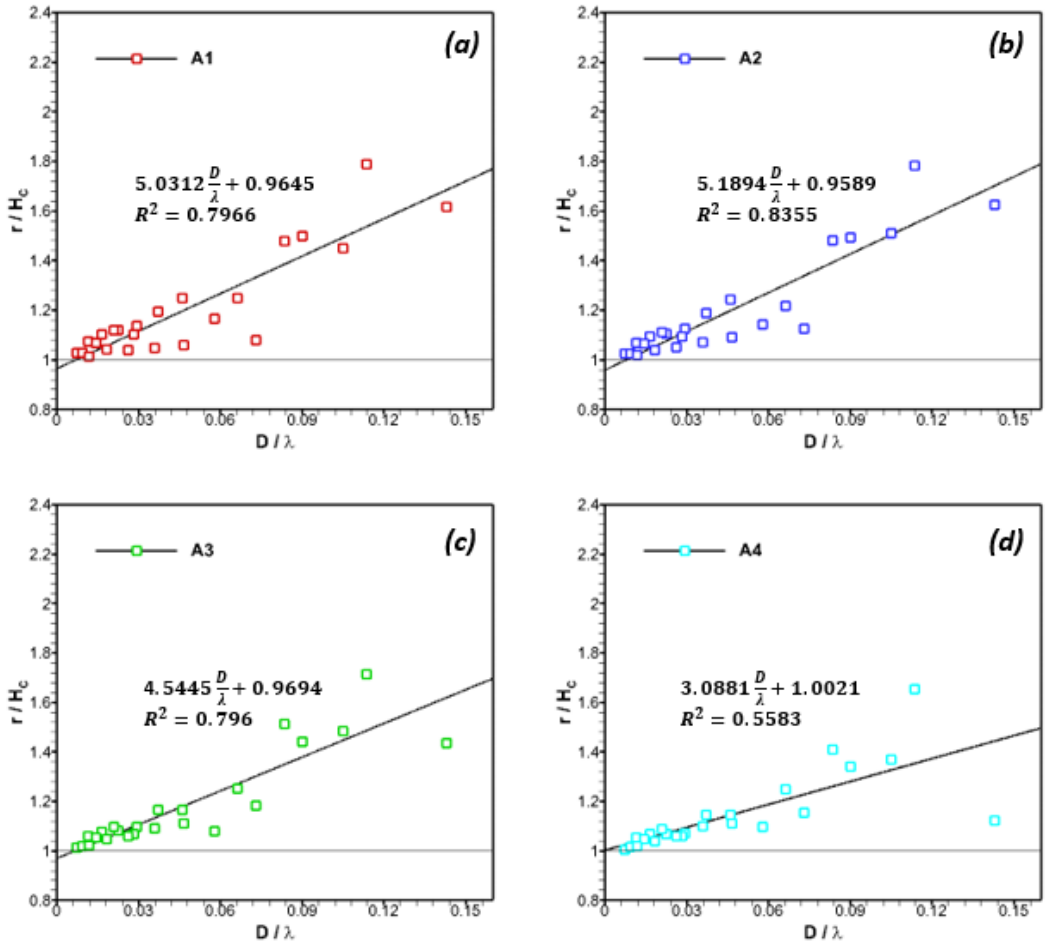

Figure 8.10 Wave run-up estimation based on the ratio of column diameter to wave length in the fore column (A)

In the fore column (A), it is apparent that the wave run-up values are not different largely from the linear approximation for the relatively small ratios, indicating that they have almost proportional relationship with small errors. On the other hand, the larger the diameter of the column, the higher the degree of scattering, which naturally causes an error with the estimated equation, as can be projected. It may be attributed to the fact that there is a direct influence by the reflected wave on values by the horizontal column size, which we have known intuitively.

Compared to the fore column (A), it is observed that the linear approximation at the aft column (B) has a significantly larger inclination value. This is because, as

shown by the analysis performed earlier, the maximum wave elevation was higher in the aft column. In addition, for the small ratios, it can be seen that the wave run-up values were lower than straight line, which is due to the sudden increase in the larger diameter range. This means the linear approximation does not fully take into account the non-linear characteristics, and even scattering.

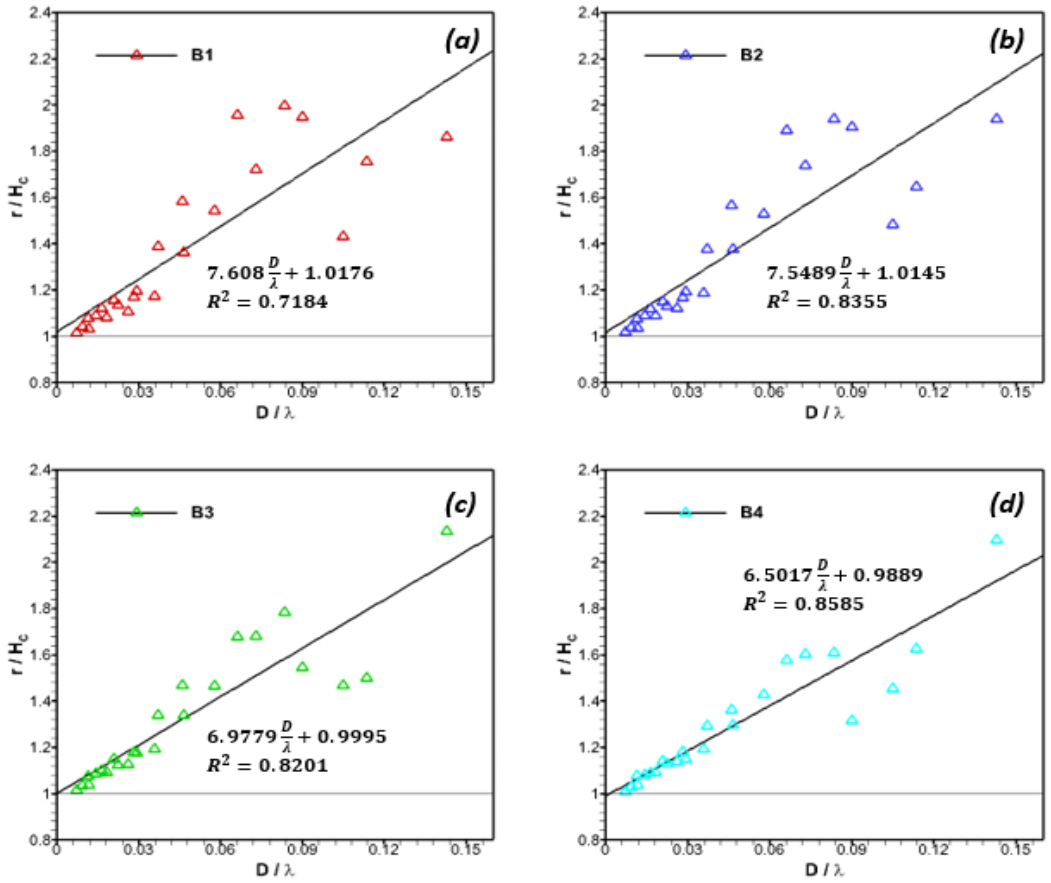

Figure 8.11 Wave run-up estimation based on the ratio of column diameter to wave length in the aft column (B)

To summarize, the maximum wave run-up values (r) within one radius can be calculated roughly from the estimated equation through linear regression analysis. The approximate expression under regular wave condition is as follows.

$$\frac{r}{H_C} = C_1 \frac{D}{\lambda} + C_2 \quad (C_2 \approx 1.0)$$

where C_1 can be chosen from 3.09 to 5.19 on the fore, and 6.50 to 7.61 on the aft column. For C_2, it is physically reasonable to have a value close to 1.

8.4 Part 3

8.4.1 A model with different drafts

The main contents of part 3 are focused on the magnitude of wave run-up depending on draft conditions. As analysed in part 2, now that the 'Up' model clearly showed the highest value (about 2.2) on aft column, this model was adopted as the fixed reference model for the draft variation. The detailed information on this study is briefly given in the following Table 8.7.

Table 8.7 Different draft conditions about 'Up' model

	Up	-3	-6
Draft (m)	0.328	0.298	0.268
Air gap (m)	0.252	0.282	0.312
The distance b/w Pontoon and still water level (m)	0.164	0.134	0.104

As shown in the table above, draft has been reduced at regular interval of 3 cm on the model scale. Therefore, this is associated with increasing the air gap, the distance between the lowest deck and the still water level, to ensure survivability in extreme conditions, which naturally leads to a reduction in draft. Here, the wave height (0.1 m) was kept constant with varying frequencies, which is the same wave condition as part 2 (Table 8.8).

Table 8.8 Wave conditions for part 3

Wave height H (m)	Wave frequency ω (rad/s)
0.10 m	1.65, 2.06, 2.47, 2.89, 3.30, 4.12, 4.95, 5.77

Other variables such as water depth also remained the same to entirely investigate draft influences on wave run-up around the column.

Needless to say, the deep water condition was maintained throughout part 3 simulations.

8.4.2 Results and Analysis

The graphs of the results of part 3 are presented in the same way as they were analysed earlier. Namely, the averaged-maximum wave run-up elevations are plotted depending on the wave frequency for the different drafts.

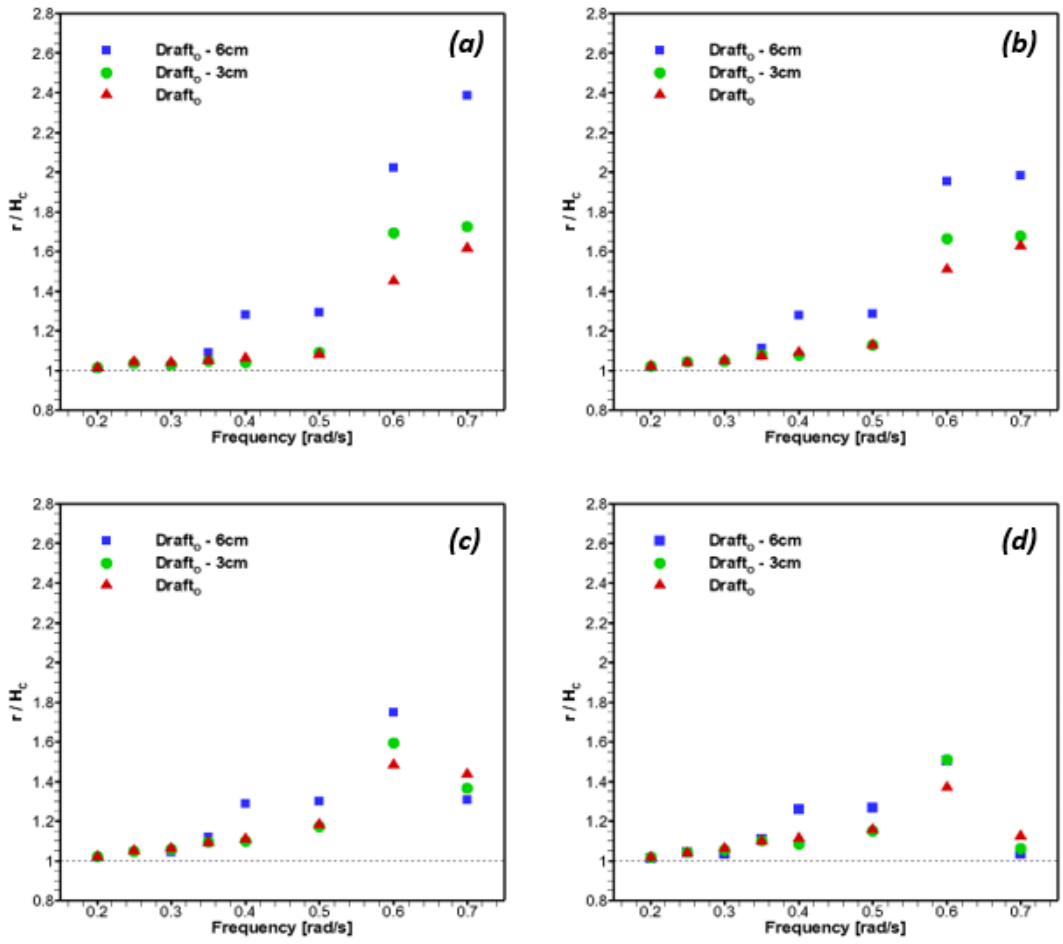

Figure 8.12 Non-dimensional wave run-up depending on the draft in fore column (A) (a) A1, (b) A2, (c) A3, (d) A4

At each location in the fore column, it is possible to see that there is a significant difference depending on the draft. Also, for values over distance from the column

from A1 to A4, the closer it is, the greater the deviation of the values by the effects of the draft variation. The maximum value here was monitored up to about 2.4 relative to the wave amplitude at the lowest draft (-6 cm) for 0.7 rad/s. It means that the magnitude of wave run-up close to fore column tends to be vulnerable to both low draft and high wave frequency as shown in Figure 8.12.

As can be seen from the analysis performed previously throughout this research, the wave run-up phenomenon around the aft column has been found to be more substantial than fore one. Expectedly, the graphs presented in the following Figure 8.13 support the explanation.

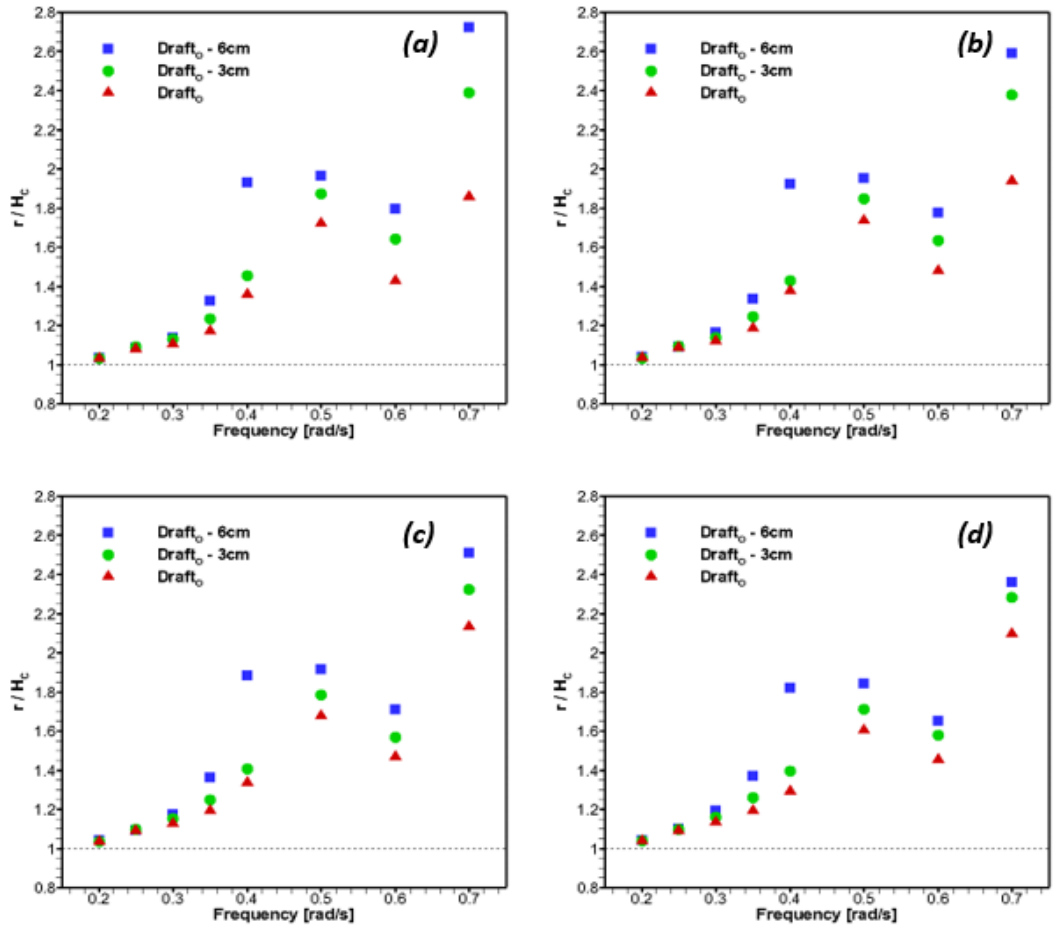

Figure 8.13 Non-dimensional wave run-up depending on the draft in aft column (B) (a) B1, (b) B2, (c) B3, (d) B4

Like the fore column, it shows the larger wave run-up value as the draft gradually reduces at the same wave probe location. In contrast to the fore column, it is found that the difference in the values along the distance within one radius from

B1 to B4 is negligible except for the highest frequency 0.7 rad/s where maximum value was increased up to approximately 2.7 (B1), showing distinct gaps depending on the locations. One of the odd features is that the value appears to be out of keeping with trend in the lowest draft at 0.4 rad/s. Comprehensively, the distance between still water level (SWL) and pontoon, as well as low draft and high frequency may be an important factor in this nonlinear phenomenon (Figure 8.14).

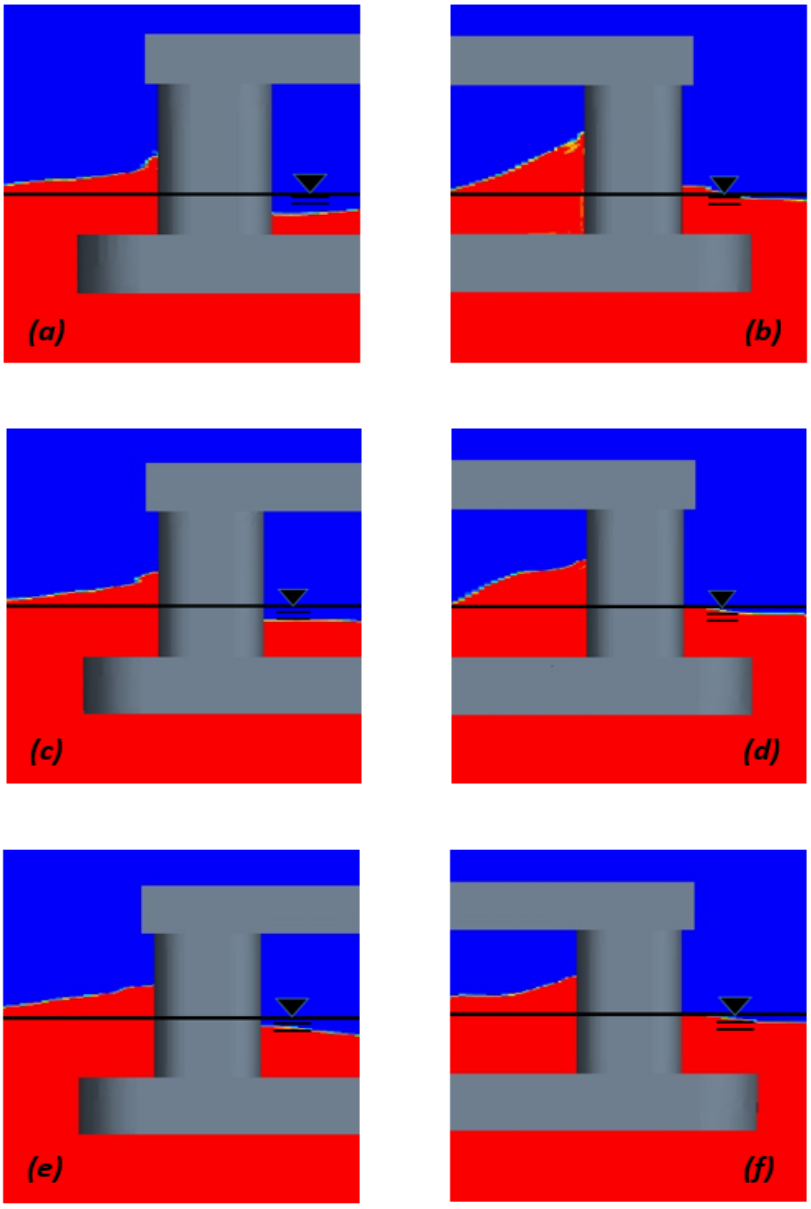

Figure 8.14 Moments when the wave elevation reaches its maximal values (a), (b) $Draft_0 - 6cm$; (c), (d) $Draft_0 - 3cm$; (e), (f) $Draft_0$ $(initial)$

9 Conclusion

The studied work in this dissertation was focused on predicting wave run-up phenomenon around the column of a semi-submersible offshore structure. A series of CFD simulations with model of a 1:68 scale ratio were carried out in the three-dimensional wave tank (NWT). The fixed model had four columns and two pontoons as whole shape. In part 1, three wave heights were considered with a wide range of the wave frequency under heading regular wave conditions. Wave elevations were monitored at four points within one radius of column in front of fore and aft column. Then, these numerical wave run-ups were compared with results based upon the potential flow model. In part 2, the models having three different hull displacement were used to investigate wave run-up differences between them for one wave height through the only CFD simulations. Aside from initial draft, two reduced draft were added to a 'Up' model with the most critical wave run-ups to analyse the influence of draft variation as well as model parts such as pontoon.

The results based on potential flow theory were compared to CFD predicted results, demonstrating that standard linear analysis tended to underestimate wave run-up values for the steep wave, as can be expected. The run-up values were much more sensitive to both distance from the wall and wave steepness in aft column. As part 2 of this study, the hull displacement has been varied and models with maximum value for each column were different; aft column (up) showed a value of about 2.2, while the fore column (original) was 1.8 under the same wave height. From these results, a simplified estimation formula with wave parameter and column diameter was derived, which can be used to rapidly calculate the wave run-up magnitude roughly in the initial design phase. For draft as a new variable, the wave run-up value generally became larger as draft was reduced. In particular, on the fore column, the influence of draft on locations in front of wall was remarkable, but not on the aft column where the maximum value of up to 2.7 compared to the incident wave amplitude was monitored in the lowest draft and highest frequency. The reduced distance b/w SWL and pontoon could be reason to rise wave run-up.

10 Future work

A semi-submersible platform has been typical floating offshore structure in line with requirements of the deeper ocean in oil & gas industry. This research has addressed wave and structure interaction as one of the complicated and demanding tasks. Due to the reasons mentioned above for this problem, it has been difficult and uncertain to estimate the extent of wave run-up elevation; especially close to the column wall, which can be concerned with evaluation of air gap further.

In terms of floating structure, motions should be normally taken into account to accurately understand relevant hydrodynamic problem. According to lots of researches conducted previously, the motion responses such as heave, pitch, roll have been known for acting favourably, reducing the maximum wave elevation under and around this type of platform. Also, irregular wave using JONSWAP spectrum was considered to investigate wave run-up with comparison of results for regular wave. In this research, for the only fixed situation due to the limitations of computation capability, maximum wave elevation within one radius from column wall was examined. The results from panel model (Genie) established by use of Wadam based on potential flow theory were compared to CFD predicted results, demonstrating that standard linear analysis tended to underestimate wave run-up values for the steep wave, as can be expected. This fact has been known very well over a decade in this field. Thus, for the purpose of considering not only the first order but higher-order than the second, various in-house codes have been developed to improve approximation about this nonlinear phenomenon.

In the future, the wave run-up for floating condition with free motions will need to be studied using both nonlinear CFD simulation and second-order potential program to obtain more practical outcome to be applied for probable situations. Now that the structure model was fixed and tested under the only heading regular wave, a variety of incident wave directions would be also a significant variable regarding this topic afterward. Furthermore, an overall evaluation of the air gap under deck can be carried out in different locations. In view of structural design, rapid impact pressure induced by wave can provide useful information with loads. Simultaneously, with aspects

presented above, the effects depending on the systematic variation of main particulars of semi-submersible will be able to be analysed, which would be definitely worth contributing the advancement of offshore hydrodynamics, even emerging offshore wind energy field. Obviously, with the suitable and efficient CFD tool Star-CCM+, a lot of ocean engineering problems would be solved and more contributions to the design of the offshore structure would be achieved.

Reference

ARNOTT, A., GREATED, C., INCECIK, A. & MCLEARY, A. 1998. An investigation of extreme wave behaviour around a model TLP. *International Journal of Offshore and Polar Engineering,* 8.

BÜCHMANN, B., SKOURUP, J. & CHEUNG, K. F. 1998. Run-up on a structure due to second-order waves and a current in a numerical wave tank. *Applied Ocean Research,* 20**,** 297-308.

CAO, H., ZHA, J. & WAN, D. Numerical simulation of wave run-up around a vertical cylinder. The Twenty-first International Offshore and Polar Engineering Conference, 2011. International Society of Offshore and Polar Engineers.

CHA, K.-J., JUNG, J.-H., SEO, K.-C. & KOO, B.-G. 2016. *A Numerical Simulation of Wave Run-up Around Circular Cylinders in Waves*.

DANMEIER, D. G., SEAH, R. K., FINNIGAN, T., RODDIER, D., AUBAULT, A., VACHE, M. & IMAMURA, J. T. Validation of wave run-up calculation methods for a gravity based structure. ASME 2008 27th International Conference on Offshore Mechanics and Arctic Engineering, 2008. American Society of Mechanical Engineers, 265-274.

HAIDER, J. 2013. *Numerical Modelling of Evaporation and Condensation Phenomena-Numerische Modellierung von Verdampfungs-und Kondensationsph änomenen.* Universität Stuttgart.

HANEY, J. P. & HERBICH, J. B. 1982. Wave flow around thin piles and pile groups. *Journal of Hydraulic Research,* 20**,** 1-14.

IWANOWSKI, B., LEFRANC, M. & WEMMENHOVE, R. CFD simulation of wave run-up on a semi-submersible and comparison with experiment. ASME 2009 28th International Conference on Ocean, Offshore and Arctic Engineering, 2009. American Society of Mechanical Engineers, 19-29.

KAZEMI, S. & INCECIK, A. Experimental study of air gap response and wave impact forces of a semi-submersible drilling unit. 25th international conference on offshore mechanics and arctic engineering, 2006. American Society of Mechanical Engineers, 65-70.

KIM, J., O'SULLIVAN, J. & READ, A. Ringing analysis of a vertical cylinder by Euler overlay method. ASME 2012 31st International Conference on Ocean, Offshore and Arctic Engineering, 2012. American Society of Mechanical Engineers, 855-866.

KIM, N., NAM, B. W., CHO, Y., SUNG, H. G. & HONG, S. Y. 2014. Experimental Study of Wave Run-up on Semi-submersible Offshore Structures in Regular Waves. *Journal of Ocean Engineering and Technology,* 28**,** 6-11.

KRIEBEL, D. Wave Amplification and Air Gap Tests on a MOB Module.

KRIEBEL, D. L. 1993. Nonlinear runup of random waves on a large cylinder.

KRISTIANSEN, T., BAARHOLM, R., RØRTVEIT, G. J., HANSEN, E. W. & STANSBERG, C. T. Kinematics in a diffracted wave field: particle image velocimetry (PIV) and numerical models. ASME 2005 24th International Conference on Offshore Mechanics and Arctic Engineering, 2005. American Society of Mechanical Engineers, 827-835.

KRISTIANSEN, T., BAARHOLM, R. & STANSBERG, C. T. Validation of second-order analysis in predicting diffracted wave elevation around a vertical circular cylinder. The Fourteenth International Offshore and Polar Engineering Conference, 2004. International Society of Offshore and Polar Engineers.

LEE, S.-K., YU, K. & HUANG, S. C. CFD study of air-gap and wave impact load on semisubmersible under hurricane conditions. ASME 2014 33rd International Conference on Ocean, Offshore and Arctic Engineering, 2014. American Society of Mechanical Engineers, V007T12A019-V007T12A019.

MATSUMOTO, F. T., WATAI, R. A., SIMOS, A. N. & FERREIRA, M. D. 2013. Wave run-up and air gap prediction for a large-volume semi-submersible platform. *Journal of Offshore Mechanics and Arctic Engineering,* 135**,** 011302.

MCCAMY & FUCHS 1954. Wave forces on piles: a diffraction theory. Tech. Memo No. 69, U.S. Army Corps of Engrs, 1954.

MORRIS-THOMAS, M. & THIAGARAJAN, K. 2004. The run-up on a cylinder in progressive surface gravity waves: harmonic components. *Applied Ocean Research,* 26**,** 98-113.

NIEDZWECKI, J. & HUSTON, J. 1992. Wave interaction with tension leg platforms. *Ocean Engineering,* 19**,** 21-37.

NIEDZWECKI, J. M. & DUGGAL, A. S. 1992. Wave runup and forces on cylinders in regular and random waves. *Journal of Waterway, Port, Coastal, and Ocean Engineering,* 118**,** 615-634.

NIELSEN, F. G. 2003. Comparative study on airgap under floating platforms and run-up along platform columns. *Marine structures,* 16**,** 97-134.

REPALLE, N., THIAGARAJAN, K. & MORRIS-THOMAS, M. CFD simulation of wave run-up on a spar cylinder. 16th Australasian Fluid Mechanics Conference (AFMC), 2007. School of Engineering, The University of Queensland, 1091-1094.

SHAN, T.-B., YANG, J.-M., LI, X. & XIAO, L.-F. 2011. Experimental investigation on wave run-up characteristics along columns and air gap response of semi-submersible platform. *Journal of Hydrodynamics, Ser. B,* 23**,** 625-636.

SIMOS, A. N., FUJARRA, A. L., SPARANO, J. V., UMEDA, C. H. & ROSSI, R. R. Experimental evaluation of the dynamic air gap of a large-volume semi-submersible platform. 25th International Conference on Offshore Mechanics and Arctic Engineering, 2006. American Society of Mechanical Engineers, 393-399.

TRULSEN, K. & TEIGEN, P. Wave scattering around a vertical cylinder: fully nonlinear potential flow calculations compared with low order perturbation results and experiment. ASME 2002 21st International Conference on Offshore Mechanics and Arctic Engineering, 2002. American Society of Mechanical Engineers, 359-367.

XIAO, X., TEZDOGAN, T. & INCECIK, A. Numerical study on wave run-up height and depression depth around a vertical circular cylinder at Various Froude numbers. Techno-Ocean (Techno-Ocean), 2016. IEEE, 618-623.

YANG, I.-J., LEE, Y.-G. & JEONG, K.-L. 2015. Numerical simulation of the free surface around a circular column in regular waves using modified marker-density method. *International Journal of Naval Architecture and Ocean Engineering,* 7**,** 610-625.

ZHANG, X., SONG, X., YUAN, Z. & YOU, Y. 2017. Global motion and airgap computations for semi-submersible floating production unit in waves. *Ocean Engineering,* 141**,** 176-204.

International Towing Tank Conference (ITTC), 2011b. Practical guidelines for ship CFD applications. In: Proceeding of the 26th ITTC.

CD-Adapco, 2017. Star-CCM + Version 12.02.010 User Guide